UNIVERSIDADE FEDERAL DO PARANÁ

JAQUELINE DOS SANTOS SILVA

# PREDICTION OF COMMUNICATION SIGNAL STRENGTH WITH UAVS USING ARTIFICIAL NEURAL NETWORKS

CURITIBA

2024

JAQUELINE DOS SANTOS SILVA

# PREDICTION OF COMMUNICATION SIGNAL STRENGTH WITH UAVS USING ARTIFICIAL NEURAL NETWORKS

Requisito parcial ao título de Mestre em Engenharia Elétrica pelo Programa de Pós-Graduação em Engenharia Elétrica (PPGEE) do Setor de Tecnologia da Universidade Federal do Paraná (UFPR).

Orientador: Prof. Dr. Evelio Martín García Fernández
Coorientador: Prof. Dr. Alessandro Zimmer

CURITIBA

2024

DADOS INTERNACIONAIS DE CATALOGAÇÃO NA PUBLICAÇÃO (CIP)
UNIVERSIDADE FEDERAL DO PARANÁ
SISTEMA DE BIBLIOTECAS – BIBLIOTECA DE CIÊNCIA E TECNOLOGIA

Silva, Jaqueline dos Santos
Prediction of communication signal strength with uavs using artificial neural networks / Jaqueline dos Santos Silva. – Curitiba, 2024.
1 recurso on-line : PDF.

Dissertação (Mestrado) - Universidade Federal do Paraná, Setor de Tecnologia, Programa de Pós-Graduação em Engenharia Elétrica.

Orientador: Evelio Martín García Fernández
Coorientador: Alessandro Zimmer

1. Redes neurais(Computação). 2. Sistemas de comunicação sem fio. 3. Drone. I. Universidade Federal do Paraná. II. Programa de Pós-Graduação em Engenharia Elétrica. III. García Fernández, Evelio Martín. IV. Zimmer, Alessandro. V. Título.

Bibliotecário: Leticia Priscila Azevedo de Sousa CRB-9/2029

MINISTÉRIO DA EDUCAÇÃO
SETOR DE TECNOLOGIA
UNIVERSIDADE FEDERAL DO PARANÁ
PRÓ-REITORIA DE PESQUISA E PÓS-GRADUAÇÃO
PROGRAMA DE PÓS-GRADUAÇÃO ENGENHARIA ELÉTRICA - 40001016043P4

# TERMO DE APROVAÇÃO

Os membros da Banca Examinadora designada pelo Colegiado do Programa de Pós-Graduação ENGENHARIA ELÉTRICA da Universidade Federal do Paraná foram convocados para realizar a arguição da dissertação de Mestrado de **JAQUELINE DOS SANTOS SILVA** intitulada: **Prediction of Communication Signal Strength with UAVs using Artificial Neural Networks**, sob orientação do Prof. Dr. EVELIO MARTÍN GARCÍA FERNÁNDEZ, que após terem inquirido a aluna e realizada a avaliação do trabalho, são de parecer pela sua APROVAÇÃO no rito de defesa.

A outorga do título de mestra está sujeita à homologação pelo colegiado, ao atendimento de todas as indicações e correções solicitadas pela banca e ao pleno atendimento das demandas regimentais do Programa de Pós-Graduação.

Curitiba, 19 de Agosto de 2024.

Assinatura Eletrônica
20/08/2024 13:54:20.0
EVELIO MARTÍN GARCÍA FERNÁNDEZ
Presidente da Banca Examinadora

Assinatura Eletrônica
20/08/2024 13:42:57.0
ANDREI CAMPONOGARA
Avaliador Interno (UNIVERSIDADE FEDERAL DO PARANÁ)

Assinatura Eletrônica
20/08/2024 14:00:33.0
SAMUEL BARALDI MAFRA
Avaliador Externo (INSTITUTO NACIONAL DE TELECOMUNICAÇÕES)

Assinatura Eletrônica
20/08/2024 14:34:06.0
LUIS HENRIQUE ASSUMPÇÃO LOLIS
Avaliador Interno (UNIVERSIDADE FEDERAL DO PARANÁ)

*I dedicate this thesis to all those who have supported and inspired me throughout this academic journey.*

*To my family, for their unconditional love and constant support.*

*To my love, for your belief in me, your encouragement, and the moments of joy and understanding we have shared.*

*To my friends, for their understanding, encouraging words, and shared memories.*

*And finally, to all the scientists and researchers who came before me, whose discoveries and dedication paved the way for my own journey of knowledge.*

## ACKNOWLEDGEMENTS

This research project was conducted through the partnership between the Graduate Program in Electrical Engineering at the Federal University of Paraná and the Master's Program in International Automotive Engineering at the Technische Hochschule Ingolstadt.

I extend my gratitude to my advisors, Dr. Alessandro Zimmer and Dr. Evelio Martín García Fernández, for their guidance, shared knowledge, and patience throughout the development of this work. My sincere thanks to Professor Dr. Christian Birkner for his patience and for the opportunity to work at the CARISSMA Institute of Safety in Future Mobility.

I would like to thank Bayerisches Hochschulzentrum für Lateinamerika (BAYLAT) for the financial support, which significantly contributed to the research conducted for this thesis. Finally, I would like to express my gratitude to my colleagues at C-ISAFE for their support and collaboration throughout this journey.

*“We are here to wonder, learn, and be curious.“*

*— Vera Rubin*

## RESUMO

Reconhecendo a crescente importância dos veículos aéreos não tripulados, mais especificamente drones, nas operações de vigilância de tráfego urbano, este projeto de pesquisa busca abordar os desafios associados à comunicação sem fio em ambientes propensos a interferências no sinal de comunicação. Propõe-se o desenvolvimento de uma rede neural artificial para prever a intensidade do sinal Wi-Fi durante voos de drones, fornecendo suporte em cenários de emergência que envolvam operações de resgate em locais de acidentes de trânsito. O algoritmo desenvolvido é um perceptron multicamadas com uma camada oculta e as seguintes características de entrada: altitude, ângulo de elevação, tipo de terreno, distância entre o drone e seu controlador, velocidade e porcentagem de bateria. Para validar a confiabilidade da solução proposta, os resultados obtidos com a rede neural foram comparados com simulações de voo de drones utilizando o modelo Longley-Rice, por meio do Radio Mobile, um software amplamente utilizado para o planejamento e modelagem de redes de comunicação sem fio. Na região rural, o perceptron multicamadas obteve um RMSE de 1,95 dB, enquanto o modelo Longley-Rice mostrou um RMSE significativamente maior de 8,23 dB. Na região suburbana, o perceptron multicamadas apresentou um RMSE de 2,93 dB, em comparação com o RMSE de 10,88 dB do modelo Longley-Rice. Na região urbana, o perceptron multicamadas teve um RMSE de 2,39 dB, enquanto o modelo Longley-Rice exibiu um RMSE de 12,84 dB. Esses resultados destacam o perceptron multicamadas como uma alternativa promissora para a previsão da intensidade do sinal em voos de drones em áreas com diferentes níveis de urbanização.



**Palavras-chaves**: vant; redes neurais artificiais; previsão de trajetória; intensidade do sinal; radio-mobile.

## ABSTRACT

Recognizing the growing importance of unmanned aerial vehicles, specifically drones, in urban traffic surveillance operations, this research project aims to address the challenges associated with wireless communication in environments prone to signal interference. The development of an artificial neural network is proposed to predict Wi-Fi signal strength during drone flights, providing support in emergency scenarios involving rescue operations at traffic accident sites. The developed algorithm is a multilayer perceptron with one hidden layer and the following input features: altitude, elevation angle, terrain type, distance between the drone and its controller, speed, and battery percentage. To validate the reliability of the proposed solution, the results obtained with the neural network were compared with drone flight simulations using the Longley-Rice model, through Radio Mobile, a widely used software for planning and modeling wireless communication networks. In the rural area, the multilayer perceptron achieved an RMSE of 1.95 dB, while the Longley-Rice model showed a significantly higher RMSE of 8.23 dB. In the suburban area, the multilayer perceptron presented an RMSE of 2.93 dB, compared to the RMSE of 10.88 dB from the Longley-Rice model. In the urban area, the multilayer perceptron had an RMSE of 2.39 dB, while the Longley-Rice model exhibited an RMSE of 12.84 dB. These results highlight the multilayer perceptron as a promising alternative for predicting signal strength in drone flights in areas with varying levels of urbanization.



**Key-words**: uav; artificial neural networks; path prediction; signal strength; radio-mobile.

## LIST OF FIGURES

## LIST OF TABLES

## LIST OF ABBREVIATIONS AND ACRONYMS

| | |
|---|---|
| **AMICA** | Air Mobility for Intelligent Crash Assessment |
| **ANN** | Artificial Neural Network |
| **C-ISAFE** | CARISSMA Institute of Safety in Future Mobility |
| **CLMS** | Copernicus Land Monitoring Service |
| **EU** | European Union |
| **GPS** | Global Positioning System |
| **GUTMA** | Global UTM Association |
| **ITM** | Irregular Terrain Model |
| **IoT** | Internet of Things |
| **JSON** | JavaScript Object Notation |
| **LPWAN** | Low-Power Wide-Area Network |
| **LoRaWAN** | Long Range Wide Area Network |
| **MAE** | Mean Absolute Error |
| **MLP** | Multilayer Perceptron |
| **MSE** | Mean Squared Error |
| **NUTS** | Nomenclature of Territorial Units for Statistics |
| **RMSE** | Root Mean Squared Error |
| **RSSI** | Received Signal Strength Indication |
| **ReLu** | Rectified Linear Unit |
| **UAVs** | Unmanned Aerial Vehicles |
| **Wi-Fi** | Wireless Fidelity |

## TABLE OF CONTENTS

# 1 INTRODUCTION

Drones fall under the category of Unmanned Aerial Vehicles (UAVs) and have gained prominence due to their applications across various fields. They are particularly notable for their versatility and efficiency in areas such as agriculture, urban traffic management, and public safety, where they are integral to surveillance and emergency response operations (Shakoor et al., 2019).

Wireless communication, established in drone communication networks, provides connectivity and coverage in hard-to-reach locations, such as mountainous regions, where terrain characteristics can hinder communication, or in areas affected by natural disasters, where phone and internet infrastructure may be compromised or nonexistent. By eliminating the need for physical infrastructure installation, drones offer a flexible solution for communication scenarios in various environments (Zeng et al., 2016).

The quality of the communication signal is essential to ensure the proper functioning of drone operations, aiding in security functions such as real-time control and collision management. Such measures are essential for accident prevention and ensuring the integrity and safety of both the device and the areas over which they operate. Thus, accurate prediction of wireless communication signal quality and intensity in drone networks is essential for network planning and its components, considering their high mobility, which poses challenges for ensuring stable and reliable communication (Yang et al., 2019).

In this context, there is a balance between managing drone resources, maximizing flight duration, and energy efficiency, especially in densely populated and structurally complex urban environments. Choosing the appropriate modulation technique and communication protocol is fundamental to ensuring the effective use of available resources, considering possible signal interferences and obstacles without compromising communication. Additionally, energy efficiency is a critical aspect, as energy is a limited resource in drones (Shakoor et al., 2019).

Machine learning has emerged as a subfield of artificial intelligence, enabling new problem-solving methods. Specifically, in the context of drones, integrating machine learning techniques represents a promising and relatively unexplored horizon, offering a vast field for research and innovation. While conventional methods provide satisfactory solutions for scenarios involving terrestrial network planning, applying machine learning techniques could offer more precise results for situations where one of the communication nodes is constantly moving, due to its potential to process large volumes of data with notable speed and accuracy (Lahmeri et al., 2021).

The investigation of the effectiveness of machine learning methods in predicting Wi-Fi signal strength in drone flights is the central theme of this research, which proposes the development of an artificial neural network capable of predicting Wi-Fi (Wireless Fidelity) signal strength in drone flights. This research integrates the AMICA project (Air Mobility for Intelligent Crash Assessment) developed by the CARISSMA Institute of Safety in Future Mobility (C-ISAFE), which aims to integrate UAVs into traffic accident rescue operations to provide real-time visual information to control centers. The project focuses on the safe operation of drones from strategic bases, using advanced algorithms to identify accident scenes from an aerial perspective. The goal is to improve the coordination of rescue operations and demonstrate technical feasibility through drone tests. In this context, signal strength prediction plays a fundamental role in ensuring reliable communication between the drone and the control station in emergencies involving rescue operations.

## 1.1 OBJECTIVES

### 1.1.1 Main Objective

This project aims to predict communication signal strength in drone flights to optimize flight routes in urban environments, aiding rescue operations involving traffic accidents. To achieve this objective, the development of a multilayer perceptron and the calculation of received power with the Longley-Rice propagation model using Radio Mobile software are proposed. Finally, the signal strength results obtained by both methodologies will be comparatively analyzed.

### 1.1.2 Specific Objectives

The specific objectives of this project are:

- Deepen the understanding of essential concepts and the state of the art in artificial neural networks, focusing on Wi-Fi signal strength prediction;
- Through data preprocessing, obtain a set of telemetry data suitable for neural network training and simulation in Radio Mobile;
- Develop and refine the multilayer perceptron algorithm, including defining its architecture and hyperparameters;
- Calculate Wi-Fi signal strength values with the Longley-Rice model using Radio Mobile software;
- Obtain a more accurate artificial neural network in terms of signal strength than the results obtained through Longley-Rice terrain model simulations.

## 1.2 DOCUMENT STRUCTURE

This document is structured to include the CHAPTER 1, which aims to elucidate the aspects that contribute to the relevance of the research and its purpose, containing the Objectives section where the general and specific objectives of the project are described, clarifying the expected results at the end of the project.

The following chapter pertains to the CHAPTER 2, which aims to contextualize the reader on the fundamental concepts related to the project and the related works section that contains publications similar to and references to the state of the art for the development of this work.

Subsequently, the CHAPTER 3 describes the development stages and resources used to carry out the research project, being essential to understand how the research was conducted, from conception to execution, including the tools and methods employed to achieve the established objectives.

The CHAPTER 4 presents the obtained results of signal strength prediction with the Longley-Rice model and the multilayer perceptron. The CHAPTER 5 refers to the Conclusion and recommendations for future work.

# 2 LITERATURE REVIEW

## 2.1 WIRELESS COMMUNICATION SIGNAL

The signal strength of a wireless communication network is crucial to the system, significantly influencing reliability, transmission rate, and connection range. Signal strength is typically measured in dBm, a unit that expresses absolute power on the decibel (dB) scale, referenced to 1 milliwatt (mW) (Cheng et al., 2019).

The strength of the wireless signal can be attenuated by several factors, including the distance between the drone and the control station, the presence of obstacles such as buildings or trees, and the frequency and transmission power of the propagated signals. Interference from other wireless devices or electronic devices can also affect signal quality. Wireless signal strength is a crucial factor determining the quality of wireless communication in a network, as a strong signal ensures a fast, reliable, and stable connection, while a weak signal can result in slow speeds or connection interruptions (Cheng et al., 2019).

In summary, signal strength emerges as a fundamental element in wireless communication networks for drones, playing a fundamental role in determining the effectiveness and reliability of data transmission to the control station. In this context, the adoption of techniques that optimize flight parameters, such as altitude and elevation angle, is essential for enhancing signal strength (Cheng et al., 2019).

Propagation loss models, essential in the analysis and design of wireless communication systems, including those used in drones, can be categorized into seven distinct groups, each with its characteristics and specific applications. Basic models offer an overview of propagation loss and are useful for quick estimates and initial analyses where a detailed understanding is not critical.

On the other hand, theoretical or fundamental models are based on physical and mathematical principles, seeking to capture the underlying mechanisms of radio wave propagation, such as reflection and diffraction, providing greater accuracy than basic models.

Terrain models account for the specific characteristics of the terrain, such as mountains and buildings, and are widely used in outdoor or urban environments where the terrain significantly influences signal propagation (Phillips et al., 2013).

Supplementary models add information to other propagation loss models, possibly including factors such as atmospheric conditions and vegetation, which also affect signal propagation. Stochastic fading models deal with the random nature of signal

fading due to movements, environmental variations, and interferences. Multipath models consider the propagation of waves in real environments and are based on the theory of multipath, where the communication signal is reflected by obstacles during its path to the receiver. Finally, measurement-based models are based on actual measurement data, unlike theoretical models, and are employed to create propagation loss models that accurately reflect the specific conditions of an environment or location (Phillips et al., 2013). FIGURE 1 illustrates the main propagation loss models and their relationships.

FIGURE 1 – RELATIONAL TREE OF THE MAIN PROPAGATION LOSS MODELS.

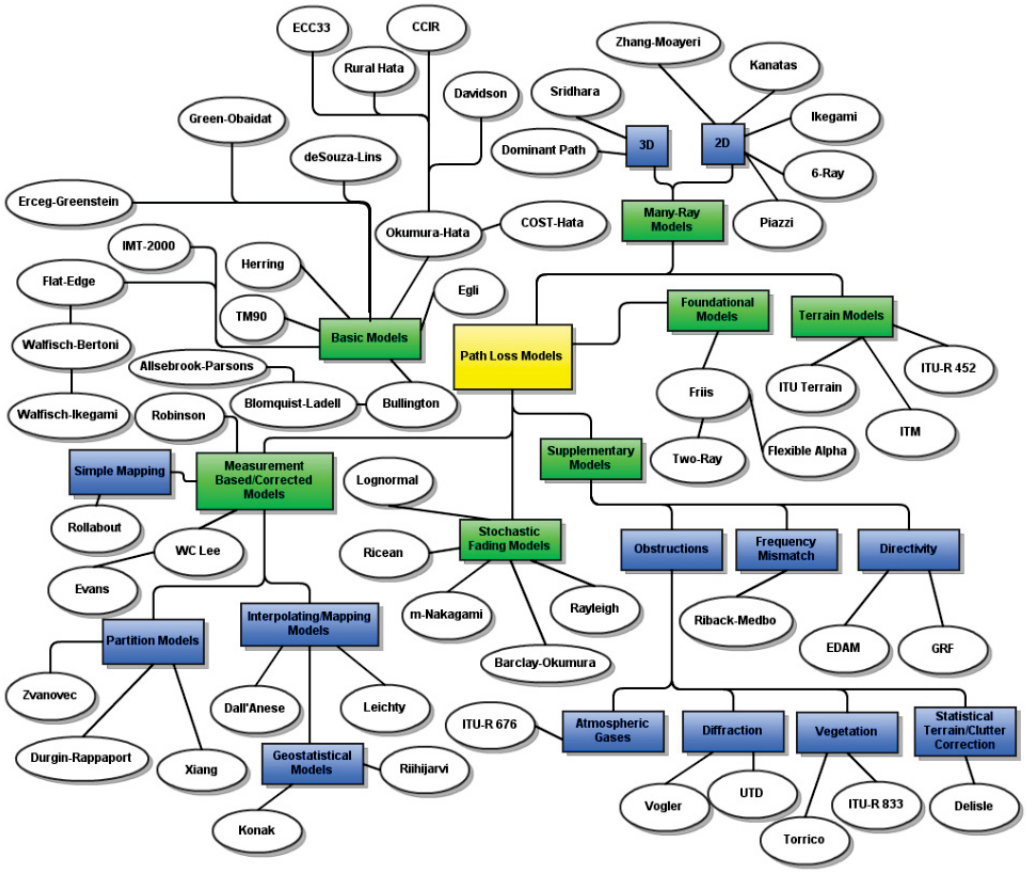


SOURCE: Adapted from (Phillips et al., 2013).

In the radio communication process, the transmitter's function is to produce a signal, which is an electromagnetic wave, and this signal is then modulated by a carrier frequency. This modulation is essential for the signal to be transmitted through space (Phillips et al., 2013).

As it propagates from the transmitter to the receiver, the signal encounters various obstacles until it is received at the receiving antenna and demodulated. These obstacles can be buildings, mountains, trees, or even atmospheric variations, each interacting with the signal causing reflection, refraction, or diffraction, which decreases the received signal strength and causes scattering and secondary waves that can interfere with the transmitted signal (Phillips et al., 2013).

The combination of these secondary waves can generate slow fading or large-scale fading, and if due to small transient obstacles and changes over time, it is called decay, fast fading, or small-scale fading (Phillips et al., 2013).

The geometry of antennas, both transmitting and receiving, plays a crucial role in determining how signals are transmitted and received. An antenna model is carefully chosen to enhance signals received from directions of interest while attenuating or minimizing signals from other directions. An omnidirectional antenna, for example, is designed to prioritize the reception of signals in the horizontal plane, meaning it can receive signals from all directions but has reduced capacity to capture signals from higher or lower vertical angles. On the other hand, a directional antenna is designed to highlight signals from a specific direction by having a defined beamwidth, which is the area where the antenna can effectively receive or transmit signals (Phillips et al., 2013).

## 2.2 LONGLEY-RICE MODEL

Propagation models assist in predicting data transmission quality, which is affected by factors such as signal loss due to physical obstacles, interference from other signals, and variations in atmospheric conditions. Understanding these factors is essential for optimizing network planning and infrastructure, aiding in the selection of suitable locations for antenna placement, and enabling the implementation of interference mitigation techniques (Cheng et al., 2019).

Parameters related to the drone, such as altitude, speed, flight direction, and elevation angle, directly impact the characteristics of the communication signal. For example, the drone's altitude may significantly influence the line of sight between the drone and the receiver, as a higher altitude can reduce physical obstructions from buildings or other structures, thereby improving signal quality. However, it can also increase the distance the signal must travel, potentially resulting in greater attenuation. The speed and direction of the drone's flight are also critical factors. The drone's elevation angle, or the tilt of its antenna, can affect the direction and intensity of the transmitted signal, influencing coverage area and reception quality. Additionally, abrupt changes in speed or flight direction can also disrupt connection stability (Cheng et al., 2019).

Flight environments also directly influence communication signal quality, which varies according to the presence of natural and urban interferences. Therefore, both the environment's characteristics and the drone's flight properties should be considered together to predict communication network quality parameters (Cheng et al., 2019).

Terrain models represent an evolution from basic models by adding the complexity of calculating diffraction losses along the path between the transmitter and receiver

due to obstacles such as mountainous terrain or buildings. Diffraction is a phenomenon that occurs when a signal interacts with physical obstacles, such as uneven terrain, mountainous formations, or urban structures, resulting in changes in the signal's trajectory and intensity. Terrain models are characterized by a more comprehensive and detailed approach, incorporating the analysis of topography and the structural characteristics of the environment (Phillips et al., 2013). FIGURE 2 shows a schematic of communication in terrain models:

FIGURE 2 – SCHEMATIC OF COMMUNICATION IN TERRAIN MODELS.

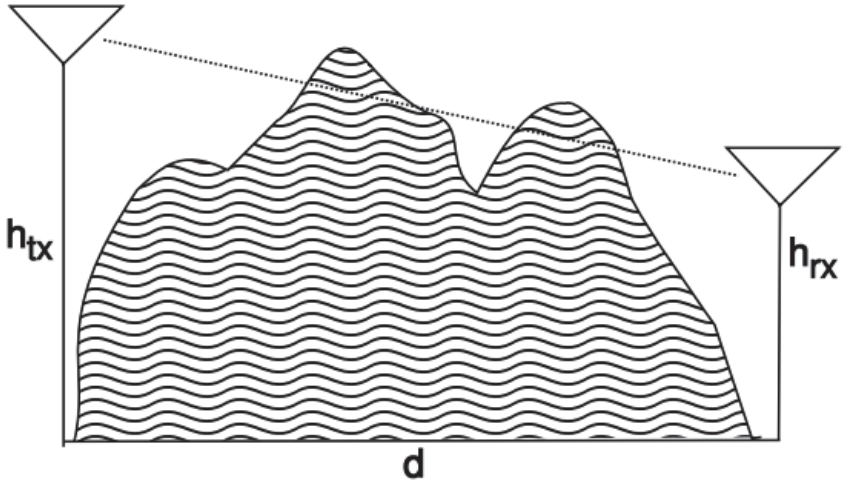


SOURCE: Adapted from (Phillips et al., 2013).

Among them, the Longley-Rice irregular terrain model, also known as ITM (Irregular Terrain Model), stands out. Recognized as one of the widely used terrain models, ITM is extensively utilized in various essential network planning tools. ITM considers a series of environmental and geographical factors, including the height and density of obstacles, signal frequency, antenna polarization, and atmospheric conditions. This allows the model to provide accurate propagation loss estimates in environments with irregular and urbanized terrain (Hufford et al., 1982).

ITM is notable for its ability to incorporate a series of complex environmental and geographical factors into its calculations, making it particularly precise and relevant for scenarios involving terrain topology. One of ITM's distinctive aspects is its ability to calculate signal loss considering diffraction caused by terrestrial obstacles. This means that the model can predict how radio waves are influenced by elements such as mountains, buildings, or other structures that can deflect or attenuate the signal.

Additionally, ITM considers the Earth's curvature in its calculations, a factor often neglected in simpler models but which can significantly impact signal propagation over long distances. These elements contribute to the model's accuracy and relevance in specific applications, despite its complexity and limitations in certain urban contexts

where the multiplicity and proximity of obstacles can compromise calculation accuracy (Hufford et al., 1982).

ITM offers two prediction modes: "area prediction"and "point-to-point."In the area prediction mode, the model uses a terrain irregularity parameter based on the interdecile range of terrain elevations, which refers to a statistical measure used to describe the variation in elevation of a specific terrain area. The process involves analyzing terrain variation by removing the top 10% and bottom 10% of elevations to obtain a more stable terrain representation.

On the other hand, the point-to-point mode employs a detailed analysis of the terrain profile between the transmitter and the receiver, using a sample of up to 600 points along the straight line connecting both. This method is particularly useful for evaluating signal loss on specific routes or in direct point-to-point connections (Hufford et al., 1982).

The model requires several parameters such as the operating frequency $f_c$ (MHz), the distance between the transmitter and receiver $d$ (m), and the heights of the transmitting and receiving antennas $h_B$ (m) and $h_M$ (m). An additional parameter, $\Delta h$ (m), indicates the roughness factor that is statistically linked to the actual heights of obstacles and to a function $\Delta h(d)$, which varies with the path distance $d$. This function $\Delta h(d)$ represents the interdecile range of terrain heights that are either above or below a fitted straight line based on elevations relative to sea level (Delisle et al., 1985).

The relationship between $\Delta h(d)$ and $\Delta h$ is expressed by:

$$\Delta h(d) = \Delta h \left[1 - 0.8 \exp(-0.02d)\right].$$

Furthermore, the model necessitates knowledge of classic parameters: $d_{L_B}$, which represents the distance from the base station to the radio horizon; $d_{L_M}$, the distance from the mobile station to the radio horizon; $\theta_{e_B}$, the horizon elevation perceived by the base station antenna; $\theta_{e_M}$, the horizon elevation perceived by the mobile station antenna; $\theta_i$, the angular distance for a non-optical path; $h_B$, the height of the base station antenna; and $h_M$, the height of the mobile station antenna.

The horizon distances in metric units are defined as:

$$d_{L_SB} = \sqrt{17h_B}, \quad d_{L_SM} = \sqrt{17h_M}.$$

The total horizon distance can be calculated as:

$$d_{L_S} = d_{L_SB} + d_{L_SM}.$$

Statistical estimates for the horizon distances are provided by:

$$d_{L_B} = d_{L_SB} \exp\left(-0.07\sqrt{\frac{\Delta h}{h_B}}\right), \quad d_{L_M} = d_{L_SM} \exp\left(-0.07\sqrt{\frac{\Delta h}{h_M}}\right),$$

with the effective antenna height defined as:

$$h_e = \begin{cases} h_B, & \text{if } h_B, h_M \geq 5m, \\ 5m, & \text{otherwise.} \end{cases}$$

The total distance between the antennas and their horizons is:

$$d_t = d_{L_B} + d_{L_M}.$$

The horizon elevation angles are calculated as follows:

$$\theta_{e_B} = \frac{0.0005}{d_{L_S B}} \left[ 1.3 \left( \frac{d_{L_S B}}{d_{L_B}} - 1 \right) \Delta h - 4 h_e \right].$$

$\theta_{e_M}$ is obtained by replacing the subscript $B$ with $M$.

The angular distance for a non-optical path is given by:

$$\theta_i = \max \left( \theta_{e_B} + \theta_{e_M} - \frac{d_t}{8495} \right) \text{ rad.}$$

The diffraction loss terms for two ideal obstacles are computed as:

$$v_{B,i} = 1.2915 \sqrt{\frac{d_L(d_i - d_L)}{d_i - d_{L,B}}}, \quad v_{M,i} = 1.2915 \sqrt{\frac{d_L(d_i - d_L)}{d_i - d_{L,B}}}.$$

The diffraction losses are defined as:

$$A(v) = 6.02 + 9v, \quad 1.0 \leq v \leq 2.4,$$

$$A(v) = 12.953 + 20 \log(v), \quad v > 2.4.$$

$$A_{k1} = A(v_{B,i}) + A(v_{M,i}), \quad A_{k2} = A(v_{B,i}) + A(v_{M,i}).$$

The path attenuation due to diffraction is expressed as:

$$L_D = m_d \times d + A_0 \quad \text{(dB)},$$

where

$$m_d = \frac{A_{k2} - A_{k1}}{d_2 - d_1}, \quad A_0 = A'_0 + A_{k2} - m_d \times d_2.$$

The clutter factor is represented by:

$$A'_0 = \min(A'_f, 15) \quad \text{(dB)},$$

where the ruggedness function is given by:

$$A'_f = 5 \log_{10} \left[ 1 + 10^{-5} \times k_h h_{B_f} f_0 \sigma(d_s) \right] \quad \text{(dB)}.$$

$$\sigma(d) = 0.78 h(d) \exp \left\{ -0.5 \left[ \Delta h(d)^{1/4} \right] \right\} \quad \text{(m)}.$$

## 2.3 ARTIFICIAL NEURAL NETWORKS

An Artificial Neural Network (ANN) is employed in a variety of tasks, including image and speech recognition, natural language processing, and autonomous vehicles. An ANN is widely implemented in drones for a range of applications, such as object recognition, image classification, path planning, and autonomous navigation.(Lahmeri et al., 2021).

For applications involving drones, ANNs can assist in tasks such as object recognition, image classification, route planning, and autonomous navigation, enabling operation in complex environments, performing functions ranging from urban monitoring to package delivery (Lahmeri et al., 2021).

An ANN is a class of machine learning algorithms modeled after the structure and function of the human brain. They consist of interconnected processing nodes called artificial neurons, which resemble biological neurons in their basic function, processing information by performing calculations on inputs and assigning results to other neurons (Lahmeri et al., 2021).

The learning process in an ANN involves combining received inputs, weighted by weights, which are used to assign an importance value to each neuron's inputs. The neurons are organized into layers, with the input layer responsible for receiving raw data, the hidden layers processing the data, and the output layer providing the network's result. During training, the neural network adjusts the weights based on the backpropagation process, which minimizes the difference between the network's output and the expected output. This procedure is repeated, allowing the network to become progressively more accurate in its predictions or classifications (Lahmeri et al., 2021). The weights adjust as follows:

$$w_i \leftarrow w_i + \Delta w_i, \tag{2.1}$$

$$\Delta w_i = \eta(t - o)x_i, \tag{2.2}$$

where $w_i$ is the weight associated with input $x_i$, $\Delta w_i$ is the change in weight $w_i$, $\eta$ is the learning rate, $t$ is the target output for the current training example, $o$ is the output generated by the perceptron, and $x_i$ is the input $i$ (Mitchell, 1997).

The ability to produce suitable outputs for inputs not previously mapped in training confers ANNs the ability to generalize, which aids in their effectiveness in developing models for prediction problems due to their flexibility and capacity to learn the underlying relationships between inputs and outputs of a process without requiring explicit knowledge of how these variables are related (Eichie et al., 2017).

Within the context of artificial neural networks, a neuron's ability to operate linearly or non-linearly is fundamental to the system's performance and functionality. The neural network is composed of the interconnection of multiple non-linear neurons, resulting in a globally non-linear system, which contributes to the network's ability to process and model complex dynamics (Haykin, 2008).

The adaptability of neural networks allows the weights to be adjusted in response to environmental changes, facilitating the network's easy reconfiguration to address variations in operational conditions and real-time adaptation in non-stationary environments (Haykin, 2008). Fault tolerance is a property of neural networks that ensures operational continuity under adverse conditions due to the distributed information and processing throughout the network (Haykin, 2008).

An artificial neuron is an information processing unit in artificial neural networks, consisting of three basic elements: a set of connections, a summing function, and an activation function. FIGURE 3 exemplifies the model of an artificial neuron.

FIGURE 3 – MODEL OF AN ARTIFICIAL NEURON.

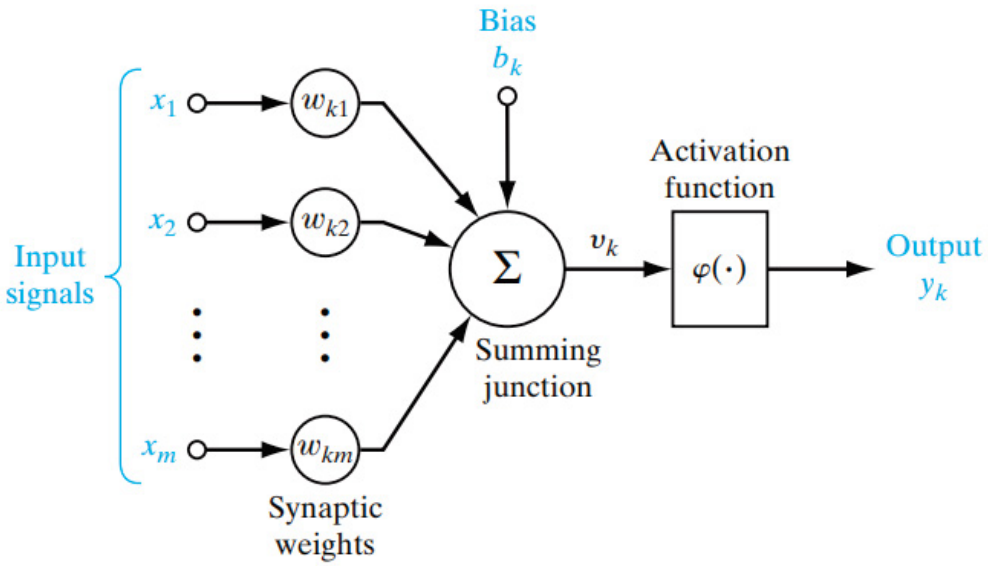


SOURCE: Adapted from (Haykin, 2008).

The input signals are weighted by weights, which assign an importance value to each input parameter and are combined linearly through a summing function. The activation function is used to limit the neuron's output amplitude to a predefined finite range. The bias function allows greater adaptability and flexibility to the neural network and enables the displacement of the activation function (Haykin, 2008).

An artificial neuron can be mathematically described as:

$$u_k = \sum_{j=1}^{m} w_{kj} x_j, \tag{2.3}$$

and:

$$y_k = \phi(u_k + b_k), \tag{2.4}$$

where $x_1, x_2, \ldots, x_m$ are the input signals, $w_{k1}, w_{k2}, \ldots, w_{km}$ are the weights of neuron $k$, $u_k$ is the output of the linear combiner, $b_k$ is the bias, $\phi(\cdot)$ is the activation function, and $y_k$ is the neuron's output signal.

Learning processes in neural networks are classified into two main categories: supervised learning and unsupervised learning. Supervised learning is characterized by adjusting the neural network's parameters based on a predefined dataset with input and output examples.

On the other hand, unsupervised learning subdivides into unsupervised learning, where the neural network identifies intrinsic patterns in the input data without using predefined outputs, and reinforcement learning, characterized by adjusting the model based on the results of the network's executions without using previously provided data.

In neural networks, the activation function gives the network the ability to represent complexities and non-linear patterns in the data. Except for the input layer, which receives the raw data, all layers of a neural network, including the hidden layers and the output layer, use an activation function. The activation function is essentially a mathematical transformation applied to the output of each neuron, capable of introducing non-linearity, allowing the network to learn and model complex relationships (Ramchoun et al., 2016b).

Among the most widespread activation functions are rectified linear unit (ReLU), hyperbolic tangent, and sigmoid. The ReLU activation function is used to limit the output values of neurons, allowing only positive results. The ReLU function is widely used to introduce non-linearity into the model and is mathematically defined by the equation below:

$$f(x) = \max(0, x), \tag{2.5}$$

where $f(x)$ is the function's output for an input $x$, and $\max$ is the mathematical operator that returns the highest value from the set of associated values.

The hyperbolic tangent activation function is a mathematical function used in artificial neural networks. Formally, it is defined by the following expression:

$$\tanh(x) = \frac{e^x - e^{-x}}{e^x + e^{-x}}, \tag{2.6}$$

where $x$ is the input value.

This function maps input values to a range between -1 and 1, making it useful for normalizing neuron outputs in a neural network. The symmetric nature of the tanh function, centering the data around zero, aims to facilitate the learning and convergence process of the network during training.

The sigmoid activation function has an output range limited between 0 and 1 and is defined by:

$$\sigma(x) = \frac{1}{1 + e^{-x}}, \tag{2.7}$$

where $x$ denotes the input to the sigmoid function and $e$ is the base of the natural logarithm.

## 2.4 MULTILAYER PERCEPTRON

The multilayer perceptron (MLP) has a wide range of applications in classification and regression problems and is considered a fully connected class of artificial neural networks. The MLP is recognized for its fully connected structure, meaning that each neuron in one layer is connected to every neuron in the next layer, which gives the MLP the ability to model complex relationships between input and output data, making it a viable option for applications where these relationships are difficult to model analytically (Ramchoun et al., 2016b).

The architecture of the multilayer perceptron (MLP) consists of an input layer, an output layer, and one or more hidden layers. The choice of network architecture greatly influences the final convergence of the network.

In the feed-forward multilayer perceptron network, information flows only from input to output, with no feedback loops. In the MLP, neurons have connections that always direct from lower layers to higher layers. The optimization of the number of hidden layers and connections can lead to an increase in processing speed and, consequently, network efficiency. Designing these parameters according to the needs of each application is necessary (Ramchoun et al., 2016a).FIGURE 4 illustrates the structure of an MLP with one hidden layer.

The neurons in the hidden layers of an MLP network are considered feature detectors, as they process inputs through the encoding of patterns, which are then used to generate the network's output. The network's ability to produce a representation for a specific pattern from the input data set depends on the number of nodes in the hidden layer (Haykin, 2008).

As demonstrated by Cybenko (1989), using one hidden layer can simulate any continuous function, while two or more layers can approximate any function. Determining

FIGURE 4 – MLP STRUCTURE WITH ONE HIDDEN LAYER.

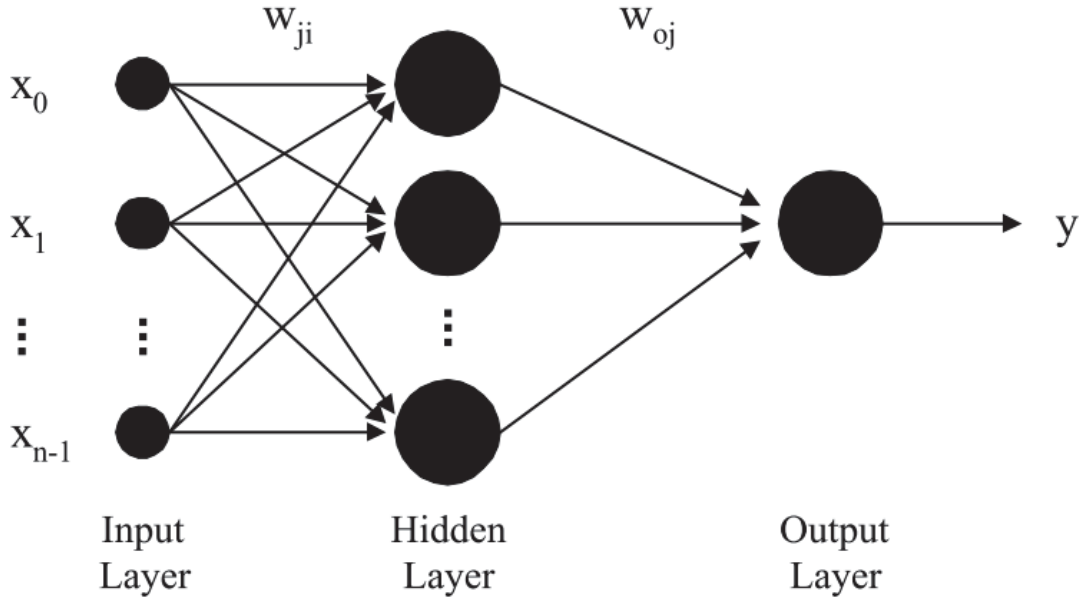


SOURCE: Adapted from Popescu et al. (2006).

the ideal number of neurons in the layer requires considering the size of the input data set, the presence of noise, the complexity of the output function, and the statistical distribution of the data during network training. The number of neurons in a hidden layer is generally chosen empirically, although methods exist to help find the best hyperparameters for the system in question.

The MLP relies on supervised backpropagation training, which is based on the gradient descent method on the error surface, where the weights are adjusted to minimize the error between the desired output and the output produced by the network. Supervised training of the MLP can be classified as static, where only the weights are adjusted, and dynamic, where the network's structure is also modified, including the number of layers and neurons.

The learning process of an MLP involves adjusting the connection weights until the neural network's output approximates the expected result. Learning is typically based on minimizing measurement errors between the network outputs and the desired outputs. The training phases of the MLP involve the forward pass to determine the network's actual output and the backward pass to update the weights (Haykin, 2008).

The supervised backpropagation training process is usually performed in cycles and starts with assigning random weights to the connections, which are adjusted to minimize the found error (Ramchoun et al., 2016b).

Loss functions quantify a model's performance by measuring the discrepancy between predicted values and actual values. A loss function maps an event or values of

one or more variables to a real number that represents the "cost"associated with the event. In an optimization problem, the goal is to minimize this loss function (Mitchell, 1997).

The basic metric used to calculate the loss function involves the observed error, which is the difference between the true and predicted values. These errors are then averaged over the entire dataset to provide a single number that represents the model's performance. The objective is to minimize these errors by finding the parameters (weights and biases) of the neural network that minimize the "loss"produced by the errors (Mitchell, 1997).

The MSE (Mean Squared Error) loss cost function is one of the most common loss functions used in machine learning, especially in regression problems. During model training, the goal is to minimize the MSE loss by adjusting the parameters of the neural network. A lower MSE loss value indicates that the model's predictions are closer to the actual values (Mitchell, 1997).

Considering the evaluation of results in regression problems, measures such as mean squared error, root mean squared error (RMSE) and the mean absolute error (MAE), along with techniques such as cross-validation and learning curve analysis, are used.

To evaluate the accuracy of the predictions and measure their precision, i.e., the number of correct predictions relative to the total number of predictions, error metrics can be calculated to measure the difference between the network's obtained values and the expected results. Among the evaluation metrics, MSE is defined as the mean of the squared error, calculated as the sum of the squared errors divided by the number of training samples, as follows:

$$\text{MSE} = \frac{1}{n}\sum_{i=1}^{n}(Y_i - \hat{Y}_i)^2, \tag{2.8}$$

where $n$ represents the total number of observations, $Y_i$ is the actual value of the $i$-th observation, and $\hat{Y}_i$ is the model's predicted value for the $i$-th observation.

RMSE is defined as the square root of the MSE value, as defined in equation 2.9, being one of the most commonly used methods for error calculation in artificial neural networks. Another widely used performance metric is the correlation matrix, which defines the linear relationship between the network's results and the expected results in regression problems.

$$\text{RMSE} = \sqrt{\frac{1}{n}\sum_{i=1}^{n}(Y_i - \hat{Y}_i)^2}, \tag{2.9}$$

MAE is a metric used to measure the accuracy of a predictive model by calculating the average absolute differences between predicted values and actual values. It is given as:

$$\text{MAE} = \frac{1}{n}\sum_{i=1}^{n}\left|Y_i - \hat{Y}_i\right|, \tag{2.10}$$

## 2.5 RELATED WORKS

The study conducted in (Behjati et al., 2021) proposes the development of an advanced agricultural monitoring system through the integration of drones, IoT (Internet of Things), and LPWAN (Low-Power Wide-Area Network). The research addresses the effectiveness of LoRaWAN (Long Range Wide Area Network) technology in providing wireless coverage in drone flights, evaluating the most accurate path loss model for the scenario under analysis. The RSSI (Received Signal Strength Indicator) measurement results demonstrated coverage exceeding 10 km, indicating the effectiveness of LoRaWAN in applications involving drones.

The irregular terrain Longley-Rice model and the ECC-33 model were considered for calculating signal strength, and although initially, satisfactory results were not obtained with these models, refinements in the ITM model significantly improved the accuracy of the obtained RSSI results, demonstrating its suitability for coverage prediction in rural environments.

Additionally, the performance of LoRaWAN was tested at different flight speeds to quantify the impact of the Doppler effect on data transmission. The tests indicated highly reliable data transmission, particularly using a spreading factor of 12, which ensured a 100% packet delivery rate at all tested speeds, while the performance of the spreading factor of 7 proved sensitive to speeds above 35 km/h. Overall, the research conducted in (Behjati et al., 2021) demonstrates the applicability of the Longley-Rice model for predicting signal strength in drone flights, especially in rural agricultural areas.

In the research presented by Saadi et al. (2022), an artificial neural network is proposed for predicting signal strength in drone flights at high altitudes. Data was collected from regions with various levels of urbanization using a standard smartphone attached to a drone to record signal strength and GPS (Global Positioning System) locations at altitudes of 10 m, 18 m, and 24 m with the drone at a fixed speed of 1 m/s.

For the development of the ANN, the data was divided into training (70%), validation (20%), and test (10%) sets. The network was trained to predict ground signal strength based on aerial measurements, using latitude, longitude, and signal strength (in dBm) as input parameters, and the predicted ground signal strength as the output.

The chosen ANN model included two hidden layers with 10 and 7 neurons, respectively.

The normalization method used was min-max, and the number of training epochs was 500, aiming to optimize the neural network's accuracy and training process to achieve an MSE of 0.001, ending the training either when the network reached the desired MSE or after 500 training steps. The number of neurons in the hidden layer varied from 1 to 20, and for each iteration, the RMSE value was calculated, resulting in the first hidden layer containing 10 neurons and the second hidden layer containing 7 neurons.

The authors opted for a regression approach where the network output represents a continuous value of signal strength, classified into four signal coverage quality categories (excellent, good, fair, and poor). The results showed that the ANN successfully predicted ground signal strength, achieving an average accuracy of 97%. Furthermore, measurements at an altitude of 10 m provided more accurate results than measurements at higher altitudes. The MSE values found were 3.91% for 10 m, 4.20% for 18 m, and 4.51% for 24 m.

The study also highlights the importance of geographic characteristics and terrain nature in predicting signal strength, as urban areas with tall buildings and various obstacles present additional complexities such as attenuation, reflection, diffraction, scattering, and signal shadowing. The study compared the neural network's effectiveness in rural and open space environments, showing that location influences signal prediction accuracy. The MSE was 2.82% in the agricultural location and 2.4% in the open space area. This study demonstrates the feasibility of effectively predicting communication signal strength in drone flights using artificial neural networks, ensuring a low-cost and efficient approach for evaluating signal coverage in hard-to-reach areas.

In Park et al. (2019), an artificial neural network model is presented for predicting propagation loss in urban environments, particularly in the 3 to 6 GHz frequency ranges. The approach is based on using a multilayer perceptron, considering rectified linear unit, hyperbolic tangent, and logistic sigmoid activation functions.

Data was collected from two urban areas in Korea, referred to as area A and area B, and segmented into training (80%), validation (10%), and test (10%) sets using uniform random sampling. The neural network had one hidden layer for the hyperbolic tangent and logistic sigmoid activation functions and up to 8 hidden layers for the ReLU activation function, as this function proved more stable with deeper network architectures.

For each architecture, configurations with different numbers of neurons were tested, with the most stable performance observed in layers with more than 20 neurons, thus 40 neurons were used for the hidden layer. The chosen input parameters were

frequency (MHz) and distance (m).

Performance analysis of the two datasets from areas A and B showed significant variations concerning the activation function used. In dataset A, the hyperbolic tangent function performed best, resulting in the lowest RMSE values for the 3.4GHz and 5.3GHz frequencies. For the 6.4GHz frequency, however, the ReLU activation function showed superior results. The results obtained in Park et al. (2019) demonstrate that the choice of activation function is a crucial factor for the performance of artificial neural networks.

The results obtained with the neural network were compared with those obtained with the COST-231 Hata model, and compared to the linear model, the neural network showed an average improvement of 8.89% and 23.26% in accuracy in areas A and B, respectively.

From the obtained results, it is possible to observe that the proposed neural network achieved better results than the COST-231 Hata model, with the hyperbolic tangent function yielding the best results. In conclusion, the article demonstrates that neural networks offer a more accurate and flexible approach for predicting propagation loss in urban environments compared to traditional signal propagation models.

In the work presented by Alsamhi et al. (2018), an artificial neural network is proposed to predict signal strength and communication channel fading to optimize service quality and data transmission in the integration of drones with IoT technologies. Signal strength is influenced by weather conditions and environmental interferences, which cause signal fading in drones flying closer to the ground. In this context, the line of sight plays a fundamental role in achieving satisfactory coverage and quality of service parameters.

Signal strength depends on distance, propagation loss, and drone flight altitude and is an essential parameter for remote drone control to maintain the flight path, receive commands from the base station, and detect objects.

In the study by Alsamhi et al. (2018), signal strength and channel fading were first calculated using established axioms and concepts in telecommunications. The Rice fading model was used to predict channel fading. Signal strength depends on transmitter and receiver parameters as well as propagation loss. Propagation models assist in predicting signal strength and propagation loss. For this study, the author used the Okumura-Hata propagation model to calculate signal strength.

In this scenario, drone flight altitude is seen as an influential parameter in predicting signal strength, as higher altitudes result in larger coverage areas and consequently increased signal interference from environmental obstacles.

For the development of the artificial neural network in Alsamhi et al. (2018), the input variables were the distance between the transmitter and receiver, drone flight

altitude, signal frequency, and propagation loss to predict signal strength and channel fading. The author proposed two observation scenarios: in the first, the drone is in motion, and its flight altitude increases from 20 meters to 200 meters. In the second scenario, the drone maintains its flight altitude while the distance between the transmitter and receiver varies.

Considering the two analyzed scenarios involving altitude, the ANN model demonstrated results closer to the expected signal strength than those found using the Hata propagation model. The study also examined the probability of line of sight relative to the drone's elevation angle in rural, suburban, and urban environments, and in this context, the ANN provided more accurate predictions than those based on Rician fading.

The authors in Alsamhi et al. (2018) demonstrated that the probability of establishing a line of sight with the drone increases as the elevation angle and altitude increase in all analyzed scenarios. The density of obstacles in the environment also influences the line of sight probability, with more urban environments requiring higher elevation angles and altitudes to achieve the same probability as rural environments.

In the research presented by Eichie et al. (2017), a comparative analysis is performed between traditional Okumura-Hata, Egli, COST-231, and Ericsson models for signal loss prediction and an artificial neural network-based model applied to calculating signal loss in wireless communications with drones. The study begins with collecting drone flight data using GPS and the Google Earth tool to classify flight areas as urban, suburban, or rural based on criteria such as population density, urban building density, building type, and spacing between buildings.

The study employs a multilayer perceptron consisting of three nodes in the input layer, which are the distance between the transmitter and receiver, transmission power, and the elevation of the measurement point above sea level. The hidden layer refers to propagation loss. The project was developed in MATLAB with the Neural Network Toolbox, with the number of neurons in the hidden layer varying from 31 to 39 in incremental steps of 2. The activation functions used were logsig, purelin, and tansig, employed to create 9 pairs of activation functions. Thus, each of the 5 different numbers of neurons was used with 9 different pairs of activation functions, resulting in 45 networks for each algorithm execution. The algorithm was run 20 times, resulting in 900 trained neural networks for performance evaluation. Performance was evaluated through MSE, adjusting weights and biases for optimization.

The results show that for rural routes, the 9-39-4 network architecture (with purelin/tansig activation functions) achieved the lowest MSE of 24.10, while for suburban routes, the 1-37-3 architecture (with tansig/purelin functions) achieved an MSE of 8.36. The correlation between the data predicted by the ANN and the actual data was 0.75 for

rural environments and 0.95 for suburban environments, indicating superior accuracy in suburban environments.

The 9-39-4 network architecture, with purelin/tansig activation functions, performed best with a minimum MSE of 24.10 for rural routes. For the suburban route, the 1-37-3 network architecture, with the tansig/purelin activation function pair, performed best with a minimum MSE of 8.36. The correlation coefficient between the measured and predicted propagation loss data by the neural network was 0.75 for the rural environment and 0.95 for suburban environments, demonstrating that the developed neural network can better predict propagation loss for suburban environments than for rural environments.

Comparatively, traditional theoretical models showed variable performance. For rural routes, the Okumura-Hata model had an RMSE ranging from 5.05 to 9.30 dB, and for suburban routes, the Egli model had an RMSE of 3.81 to 8.18 dB. However, the ANN models outperformed these results, with RMSE ranging from 3.96 to 7.07 for rural routes and 1.22 to 6.16 dB for suburban routes, outperforming the Egli, COST-231, and Ericsson models.

Next, the author compares the results obtained with the neural network and the conventional Okumura-Hata, Egli, COST-231, and Ericsson models to the measured propagation loss values in dB. For rural flight routes, the Okumura-Hata and Egli models obtained values closer to the measured results but showed low precision. Considering suburban routes, the Egli model was the closest to the actual measured values. In summary, all considered theoretical models diverged from the expected result when compared to the measured values, whereas the artificial neural network values were able to match the measured results.

The Okumura-Hata model performed best on rural routes, with RMSE ranging from 5.05 to 9.30 dB, while the Egli model, with RMSE ranging from 3.81 to 8.18 dB, performed best on suburban routes. The ANN results for rural routes outperformed the Okumura-Hata model, with RMSE ranging from 3.96 to 7.07, while the ANN-based propagation loss model for suburban routes, with RMSE ranging from 1.22 to 6.16 dB, performed better than the Egli model. The COST-231 and Ericsson models showed low accuracy in predicting path loss values for both rural and suburban scenarios.

Finally, the author concludes in Eichie et al. (2017) that among the theoretical models for predicting signal loss, the Okumura-Hata model would be more suitable for rural environments, and the Egli model would be closer to the expected results for suburban environments. When compared to the results obtained by conventional models, the artificial neural network showed a lower RMSE value, indicating it to be a good alternative for signal loss prediction scenarios.

The related works reveal the advances and challenges in using artificial neural networks for predicting signal strength in diverse drone flight environments, highlighting the ability of neural networks to overcome the limitations of signal propagation models in urbanized environments, especially in scenarios involving drone communications where one of the communication nodes is constantly moving.

The study by Saadi et al. (2022) illustrates the potential of neural networks in predicting signal strength at different altitudes, emphasizing the importance of data collection in varied environments and the influence of urbanization on predictions. The average accuracy of 97% achieved highlights the effectiveness of the approach, especially the finding that lower altitude measurements provide more accurate results, pointing to the significant impact of altitude on prediction quality.

In Park et al. (2019), the authors expand the discussion to predicting propagation loss in specific frequency bands, using an artificial neural network approach with different activation functions. The variation in performance according to the activation function highlights the importance of appropriate network parameter selection, demonstrating the applicability of neural networks in complex urban environments.

The study by Alsamhi et al. (2018) focuses on optimizing service quality in drone integrations with IoT technologies, where the neural network is used to predict signal strength and channel fading under various conditions. This study highlights the relevance of the line of sight and flight altitude, reinforcing the role of geographic and environmental characteristics in prediction effectiveness.

The research conducted by Eichie et al. (2017) offers a comparative analysis between conventional theoretical models and an artificial neural network in signal loss prediction, demonstrating the superiority of neural networks, especially in urban environments. This study reiterates the ability of neural networks to adapt to different environmental conditions, providing more accurate predictions than traditional models.

Finally, the study proposed by Behjati et al. (2021) demonstrates the applicability of using the Longley-Rice irregular terrain model for calculating signal strength in drone flights, particularly in rural environments. The application of the ITM model with LoRaWAN technologies allows the establishment of wireless coverage in extensive areas with varied and irregular topographical characteristics.

In summary, the related works highlight the potential of neural networks for predicting signal strength in various environments. The research also emphasizes the importance of selecting hyperparameters and activation functions to optimize neural network performance. Additionally, the effectiveness of the artificial neural network in urban environments in the related studies underscores the importance of considering specific environmental characteristics in network modeling and data collection.

# 3 METHODOLOGY

## 3.1 TELEMETRY DATA ACQUISITION

The telemetry data used in this research project was provided by the C-ISAFE laboratory of CARISSMA at the Technische Hochschule Ingolstadt. The Parrot ANAFI AI drone was employed for data acquisition due to its ability to operate under different climatic and environmental conditions. Flights were conducted in various regions of Germany, including urban, rural, and suburban areas, to ensure a comprehensive dataset with varied conditions.

This research project utilized telemetry data from 26 drone flights conducted in three distinct regions of Germany. No pauses were made during the flights. This ensured that the trajectory covered in each flight was continuous. The diversity and quality of the collected data are crucial for the generalization of the neural network, ensuring its robustness and reliability in different urban scenarios. The collected telemetry data includes the information listed in TABLE 1.

TABLE 1 – DESCRIPTION OF DRONE TELEMETRY DATA

| Name | Description | Unit |
|---|---|---|
| timestamp | Time of data recording in seconds since the start of the flight. | seconds |
| gps_lon | Drone GPS longitude at the time of the record. | degrees |
| gps_lat | Drone GPS latitude at the time of the record. | degrees |
| gps_altitude | Drone altitude relative to the flight's starting point. | meters |
| speed_vx | Drone speed on the x-axis. | m/s |
| speed_vy | Drone speed on the y-axis. | m/s |
| speed_vz | Drone speed on the z-axis. | m/s |
| battery_percent | Percentage of remaining battery. | % |
| battery_voltage | Total battery voltage of the drone. | volts |
| battery_cell_voltage_0 | Voltage of battery cell 0. | volts |
| battery_cell_voltage_1 | Voltage of battery cell 1 (if applicable). | volts |
| battery_cell_voltage_2 | Voltage of battery cell 2 (if applicable). | volts |
| battery_current | Battery current of the drone. | amperes |
| wifi_signal | Power received at the receiver. | dBm |
| product_gps_available | Indicates whether GPS is available (1) or not (0). | binary |
| product_gps_position_error | Estimated GPS position error in meters. | meters |
| product_gps_sv_number | Number of visible GPS satellites. | count |
| angle_phi | Drone roll angle. | degrees |
| angle_psi | Drone yaw angle. | degrees |
| angle_theta | Drone pitch angle. | degrees |
| gps_amsl_altitude | Drone altitude relative to mean sea level. | meters |

SOURCE: (Parrot Drone, 2023)

For the construction of the multilayer perceptron algorithm, the following information will be considered: altitude ('gps_amsl_altitude'), elevation angle ('angle_phi',

'angle_psi', and 'angle_theta'), speed ('speed_vx', 'speed_vy', and 'speed_vz'), battery percentage ('battery_percent'), terrain type, and distance between the drone and the controller. The terrain type and distance information were added to the dataset during the preprocessing stage.

For simulations in the Radio Mobile software, the latitude ('gps_lat'), longitude ('gps_lon'), and height information were considered. The height information was also obtained during the preprocessing stage. The flights include the specifications listed in TABLE 2.

TABLE 2 – DETAILS OF THE DRONE FLIGHTS.

| Metric | Rural Region | Suburban Region | Urban Region |
|---|---|---|---|
| Number of samples | 14048 | 12453 | 13333 |
| Maximum distance traveled (m) | 240.64 | 259.09 | 578.88 |
| Maximum height (m) | 377.57 | 412.93 | 389.75 |
| Minimum height (m) | 103.73 | 123.41 | 108.31 |

SOURCE: The Author.

## 3.2 DATA PREPROCESSING

The data preprocessing stage requires cleaning, organizing, and transforming telemetry data into a format suitable for training the neural network, which is essential for ensuring that the neural network learns efficiently and accurately, directly influencing the performance and reliability of the obtained results.

The first step in preprocessing involved converting the flight data, originally in GUTMA (Global UTM Association) format, to JSON (JavaScript Object Notation) format using the 'liblog2gutma' library provided by the drone manufacturer, Parrot. The GUTMA format is designed for drone telemetry, organizing flight data in a structured and standardized manner, facilitating interoperability between different systems and devices. However, to enhance flexibility and compatibility with the tools used, converting the telemetry data to JSON format was necessary. JSON is a widely used data structure in data science applications, known for its capacity to represent complex data in a structured and hierarchical manner.

Next, it was necessary to filter the noise in the telemetry data to ensure data integrity and accuracy. To achieve this, a statistical methodology based on dividing the data into quartiles was adopted, a technique recognized for its effectiveness in identifying and removing atypical or extreme variations.

This statistical approach involves segmenting the dataset into four equivalent parts, called quartiles. The focus of this technique is the interquartile range, which spans from the first to the third quartile (25th to 75th percentile), representing the central and

most representative section of the dataset. Values outside this range are considered outliers and are consequently excluded from the dataset to minimize noise influence.

The following equations exemplify the calculation of limits for filtering longitude data:

$$q_{\text{low\_lon}} = \text{Percentile}(gps\_lon, 0.01), \tag{3.1}$$

$$q_{\text{hi\_lon}} = \text{Percentile}(gps\_lon, 0.99), \tag{3.2}$$

where $q_{\text{low\_lon}}$ and $q_{\text{hi\_lon}}$ represent the lower and upper limits, respectively, calculated as the 1st and 99th percentiles of the longitude column ('gps_lon'). This methodology ensures that only data within a range considered normal or typical are retained, excluding extreme variations that could compromise subsequent analysis.

For a more precise identification of noise, histograms were constructed for the columns of interest present in the telemetry data, as shown in FIGURE 5 and FIGURE 6. Histograms are efficient graphical tools for visualizing data distribution, facilitating the detection of noise and unconventional patterns.

FIGURE 5 – HISTOGRAM OF THE COLUMN 'GPS_AMSL_ALTITUDE' BEFORE OUTLIER REMOVAL.

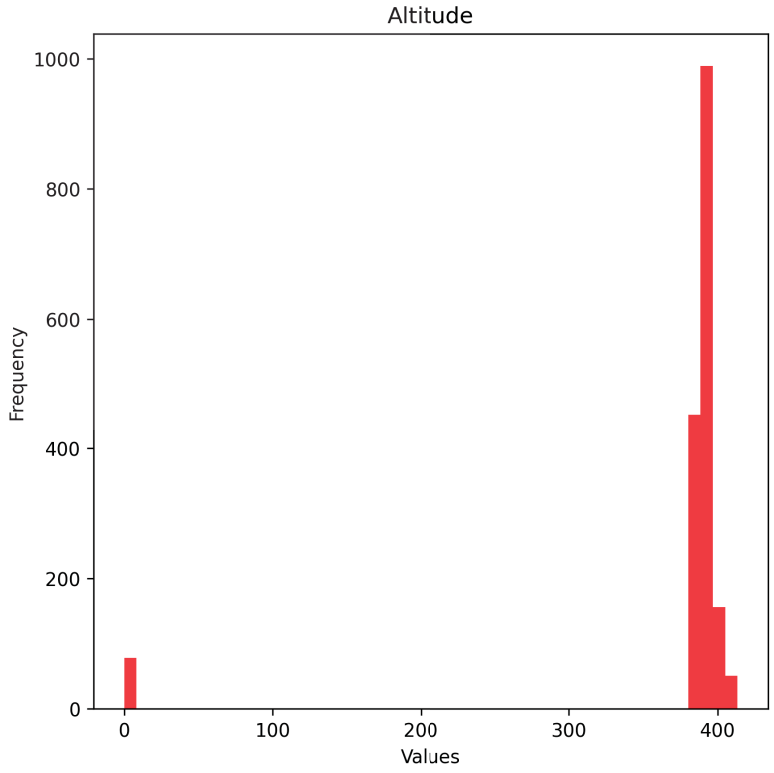


SOURCE: The Author.

FIGURE 6 – HISTOGRAM OF THE COLUMN 'GPS_AMSL_ALTITUDE' AFTER OUTLIER REMOVAL.

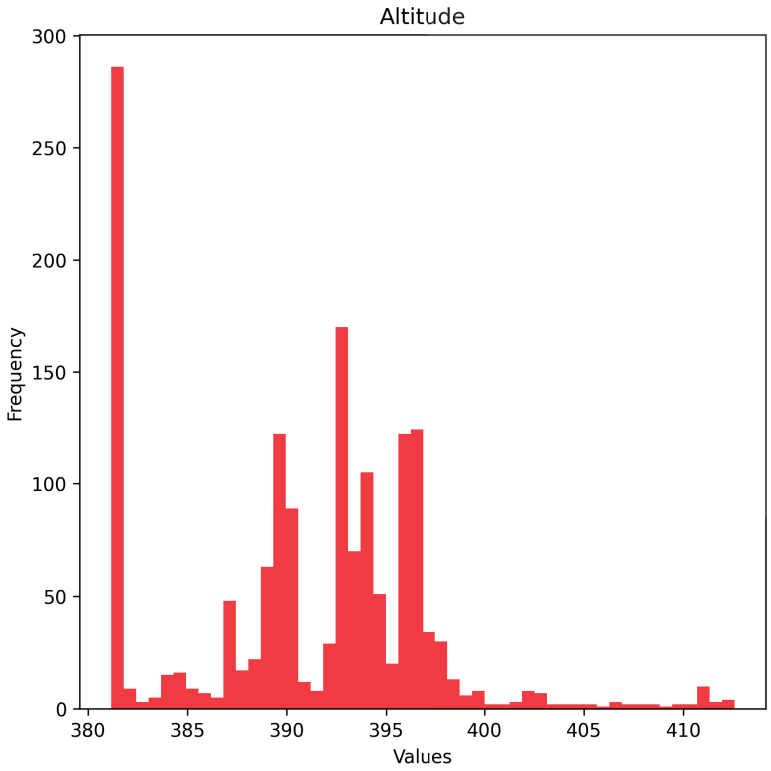


SOURCE: The Author.

FIGURE 5 illustrates that the altitude value distribution was originally concentrated around 0 and 400 meters, suggesting possible measurement errors. After outlier removal, a more uniform distribution of altitude values between 380 and 415 meters can be observed.

The terrain type information is not contained in the telemetry data provided by the drone flights. Therefore, to consider this information in the neural network, terrain type data were integrated into the telemetry data during the preprocessing stage. For this purpose, the Copernicus Land Monitoring Service (CLMS), a geospatial data repository maintained by the European Union, was utilized. The CLMS is part of the Copernicus project, an Earth observation initiative that provides detailed information on land cover and usage (Kosztra et al., 2019).

For this study, data from three specific regions, identified by the NUTS3 codes: DE211, DE219, and DE266, were selected. The NUTS3 codes form part of the NUTS classification (Nomenclature of Territorial Units for Statistics), used by the European Union for collecting, developing, and harmonizing regional statistics. It is a geographical hierarchy that divides the territories of EU member states into several layers for statistical, planning, and funding allocation purposes.

Each of the selected regions presents distinct terrain characteristics, contributing

to the diversity of the analyzed data. The DE211 region is primarily characterized by urban and industrial areas, offering a relevant context for studies in urbanized environments. The DE219 region presents a combination of agricultural land and natural areas, providing a mixed land use scenario characterizing a suburban region. On the other hand, the DE266 region is notable for its extensive forested and natural areas, offering a significant contrast with the other regions and allowing the analysis of data in predominantly rural contexts.

Integrating this information into the telemetry dataset allows the developed neural network to have a deeper understanding of the terrain characteristics over which the drone operated, which is crucial for urban and spatial monitoring applications. The types of regions mapped through the CLMS database are shown in TABLE 3.

The information on the distance between the controller and the drone is added in the preprocessing stage and plays a crucial role in calculating signal strength prediction. In this process, the first data point of each flight dataset is established as the reference point, fixing the controller's position. From this initial point, the distance between the controller and the drone at each subsequent moment of the flight is calculated. To perform this calculation, the Haversine function, a recognized mathematical method for determining the distance between two points on the Earth's surface considering its curvature, was used. It provides a more accurate estimate of the actual distance compared to a simple linear calculation.

For calculating the distance $d$ between the controller and the drone, the Haversine function is utilized. Additionally, the altitude of the flight is taken into account for a three-dimensional distance calculation.

$$d = 2R \arctan 2 \left( \sqrt{a}, \sqrt{1-a} \right), \tag{3.3}$$

where:

$$a = \sin^2 \left( \frac{\Delta\phi}{2} \right) + \cos(\phi_1) \cos(\phi_2) \sin^2 \left( \frac{\Delta\lambda}{2} \right), \tag{3.4}$$

$R$ is the radius of the Earth (approximately 6,371 kilometers), $\phi_1$ and $\phi_2$ are the latitudes of the points in radians, $\Delta\phi$ is the difference between the latitudes, and $\Delta\lambda$ is the difference between the longitudes of the two points.

To calculate the distance considering the flight altitude, the following was considered:

$$d_{3D} = \sqrt{d^2 + \Delta h_{BD}^2}, \tag{3.5}$$

TABLE 3 – CODES AND TYPES OF TERRAIN AVAILABLE IN CLMS

| **Terrain Type** | **Code** |
|---|---|
| Continuous urban areas | 111 |
| Discontinuous urban areas | 112 |
| Industrial or commercial zones | 121 |
| Road and rail networks | 122 |
| Port areas | 123 |
| Airports | 124 |
| Mining areas | 131 |
| Landfills | 132 |
| Large-scale constructions | 133 |
| Urban green spaces | 141 |
| Sports and leisure facilities | 142 |
| Arable land | 211 |
| Permanent crops | 212 |
| Permanent grasslands | 213 |
| Fruit orchards | 221 |
| Vineyards | 222 |
| Olive groves | 223 |
| Pastures | 231 |
| Agro-forestry complexes | 241 |
| Cultivated and natural vegetation interspersed | 242 |
| Broad-leaved forests | 311 |
| Coniferous forests | 312 |
| Mixed forests | 313 |
| Natural scrubland | 321 |
| Shrub and/or herbaceous vegetation areas | 322 |
| Sparse vegetation | 323 |
| Burned areas | 324 |
| Beaches, dunes, and sands | 331 |
| Rocky outcrops and scree | 332 |
| Deserts | 333 |
| Inland wetlands | 411 |
| Marshes and peat bogs | 412 |
| Estuaries | 421 |
| Coastal zones | 422 |
| Marine areas | 423 |
| Lakes and ponds | 511 |
| Reservoirs | 512 |
| Rivers and watercourses | 521 |
| Glaciers and permanent snow | 522 |

SOURCE: Kosztra et al. (2019)

where $d_{3D}$ represents the three-dimensional distance, $d$ is the distance calculated by the Haversine formula (on the Earth's surface), and $\Delta h_{BD}$ denotes the altitude difference between the two points.

To optimize the flight simulation in the Radio Mobile software, since the flight points must be manually entered, systematic sampling was used on the telemetry data, considering a 90% confidence level and a 10% margin of error. These criteria were established to ensure that the sampled data is representative of the total dataset, maintaining the precision and fidelity of the information.

To calculate the sample size $n$ in systematic sampling, considering a 90%

confidence level and a 10% margin of error, and assuming $p$ represents the proportion of interest in the dataset, the following equation was used:

$$n = \left( \frac{Z^2 \times p \times (1-p)}{E^2} \right), \tag{3.6}$$

where $Z$ represents the desired confidence level, which is 1.645 for 90%, $p$ denotes the estimated proportion of latitude, longitude, and altitude points in the dataset, $E$ is the margin of error, expressed as a decimal fraction (0.10 for 10%). The sample size $n$ is rounded to the nearest integer. After determining the sample size in systematic sampling, every $k$-th element of the set is selected, where $k$ is approximately the quotient of the total dataset divided by $n$.

To minimize the impact of instantaneous power fluctuations, the average value of the signal strength, measured in dBm, was calculated using:

$$\text{Pm} = 10^{\frac{1}{2m+1} \sum_{i=\text{idx}-s}^{\text{idx}+s} \frac{\text{wifi\_signal}_i}{10}}, \tag{3.7}$$

where idx is the index of the sampled point, $s$ represents half of the sampling interval, $m$ represents the number of observations on one side of the sampled point, ensuring the averaging is performed over $2m+1$ points, $k$ is adjusted to be an odd number to ensure that the average is calculated over a symmetric set of points around idx, and wifi_signal$_i$ are the measured power values at the points around the sampled point, covering the interval from idx $- m$ to idx $+ m$.

## 3.3 FLIGHT ROUTE SIMULATION IN RADIO MOBILE

To support the analysis of signal strength prediction considering theoretical terrain models, the Radio Mobile software was used. This software allows for modeling and predicting the behavior of radio waves in diverse environmental and topographic conditions. The software uses the Longley-Rice propagation model, which is recognized for its accuracy in predicting radio signal propagation, considering variables such as terrain topography, atmospheric conditions, operating frequency, and other relevant geographical aspects.

Among the variables considered by the Longley-Rice model, terrain topography is one of the most significant, including the height, shape, and continuity of the terrain, which can significantly affect the propagation of the communication signal. The software also considers other relevant geographical aspects, such as the presence of buildings, vegetation, and other obstacles that can reflect, absorb, or diffract the signal during transmission.

To generate a coverage map of a specific region or city, it is necessary to first extract the urban coverage and terrain elevation data of the region of interest from the databases provided by the Radio Mobile software manufacturer. After downloading and initial configurations, it is necessary to import the SRTM (Shuttle Radar Topography Mission) data and urban coverage. The SRTM data provides detailed information regarding terrain elevation, which is essential for modeling signal propagation in areas with topographic variations. The urban coverage data offers details about land cover that can affect signal propagation. The SRTM data details the urban elevation of almost the entire Earth's surface and has a resolution of 1/3 arcseconds (approximately 10 meters). The urban coverage data is provided by CLMS and has a resolution of 100 meters.

For this research project, three flights in regions with different levels of urbanization were selected to obtain results considering different levels of signal interference. Subsequently, the same flights will be used in the neural network testing phase to compare the results obtained with the two approaches. FIGURE 7, FIGURE 8, and FIGURE 9 illustrate Google Earth images of the cities of Großmehring, Heustreu, and Ingolstadt selected for simulation in Radio Mobile.

The selection criterion for the simulated flight from each region was determined by flight length, with the longest flight from each region being selected. In this context, the city of Großmehring represents the rural region with a length of 240.64 meters, Heustreu is an example of a suburban region with a flight length of 259.09 meters, and Ingolstadt is classified as an urban region with a flight length of 578.88 meters. The classification into types of environments was based on the level of urbanization exhibited in each city regarding urban coverage.

The first geographical point in the telemetry dataset of each selected flight is established as the location of the drone controller, serving as a reference for the entire simulation. For subsequent points, latitude, longitude, and height information for each location were input into Radio Mobile. The flight height added in the simulation for each point is derived through the following relation:

$$h_{\text{relative}} = h_{\text{amsl}} - e_{\text{terrain}}, \tag{3.8}$$

where $h_{\text{relative}}$ denotes the relative height of the point above the terrain, $h_{\text{amsl}}$ indicates the altitude of the point relative to sea level, and $e_{\text{terrain}}$ refers to the elevation of the terrain above sea level. The altitude information above sea level is included in the telemetry data in the 'gps_amsl_altitude' column, and the terrain elevation data are the SRTM data imported by Radio Mobile.

The latitude and longitude information is present in the telemetry data in the

FIGURE 7 – SELECTED FLIGHT IN THE GROßMEHRING REGION (RURAL AREA).


SOURCE: The Author.

FIGURE 8 – SELECTED FLIGHT IN THE HEUSTREU REGION (SUBURBAN AREA).

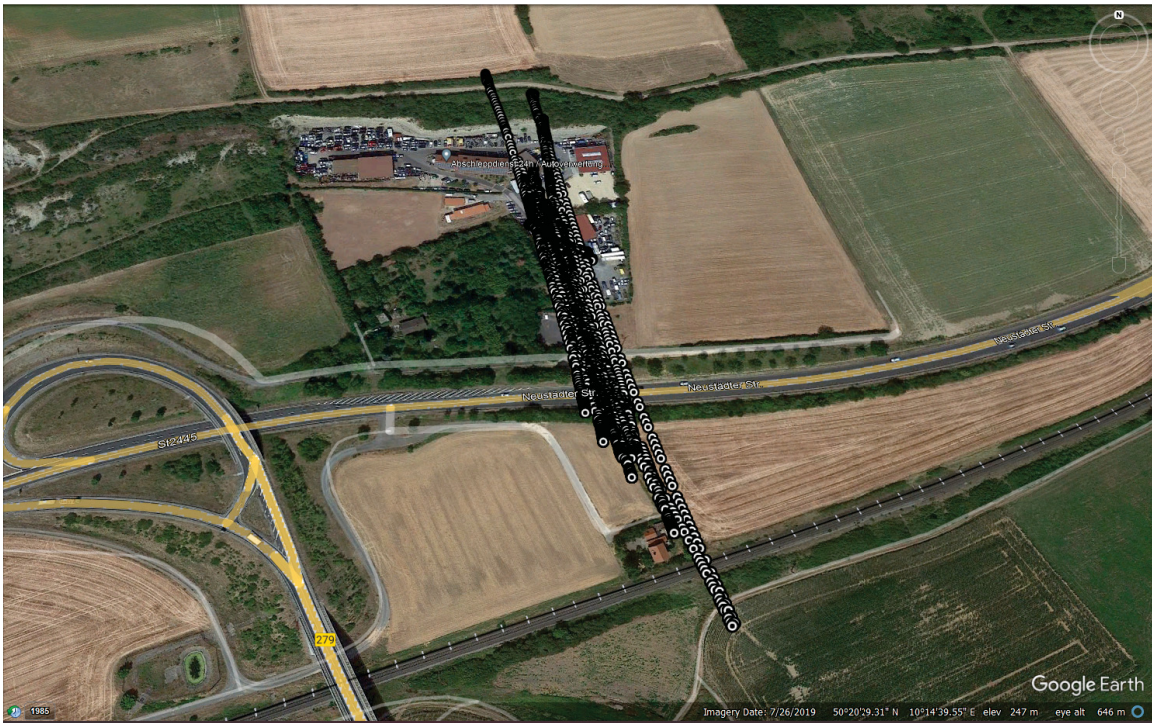


SOURCE: The Author.

'gps_lat' and 'gps_lon' columns, respectively. In the context of Radio Mobile, each geographical point is viewed as a unit, with the first unit representing to the drone controller and the second unit referring to the drone's flight points. Each of the drone's

FIGURE 9 – SELECTED FLIGHT IN THE INGOLSTADT REGION (URBAN AREA).


SOURCE: The Author.

flight points was input individually to calculate the radio link for each sampled point separately.

To represent the communication parameters and drone specifications, the network properties were calibrated to include aspects such as transmitter power, operating frequency, and antenna configurations. These adjustments are crucial for realistically simulating flight and communication conditions. Table 4 presents the configured values for the drone.

TABLE 4 – TECHNICAL SPECIFICATIONS OF THE DRONE

| Metric | Value |
|---|---|
| Transmission Power | 20 dBm |
| Operating Frequency | 2.4 GHz |
| Transmitter Antenna Gain | 3.5 dBi |
| Receiver Antenna Gain | 3.5 dBi |
| Receiver Sensitivity | -94 dBm |

SOURCE: The Author.

These parameters are configured in Radio Mobile as shown in FIGURE 10, considering a cable loss of 0.5 dB and no additional losses.

For flights conducted in Heustreu and Großmehring, which were carried out from the ground, the point corresponding to the drone controller was approximated as an antenna with a height of 0.5 meters. In contrast, for the flights conducted in

FIGURE 10 – DRONE PARAMETER CONFIGURATION IN RADIO MOBILE.

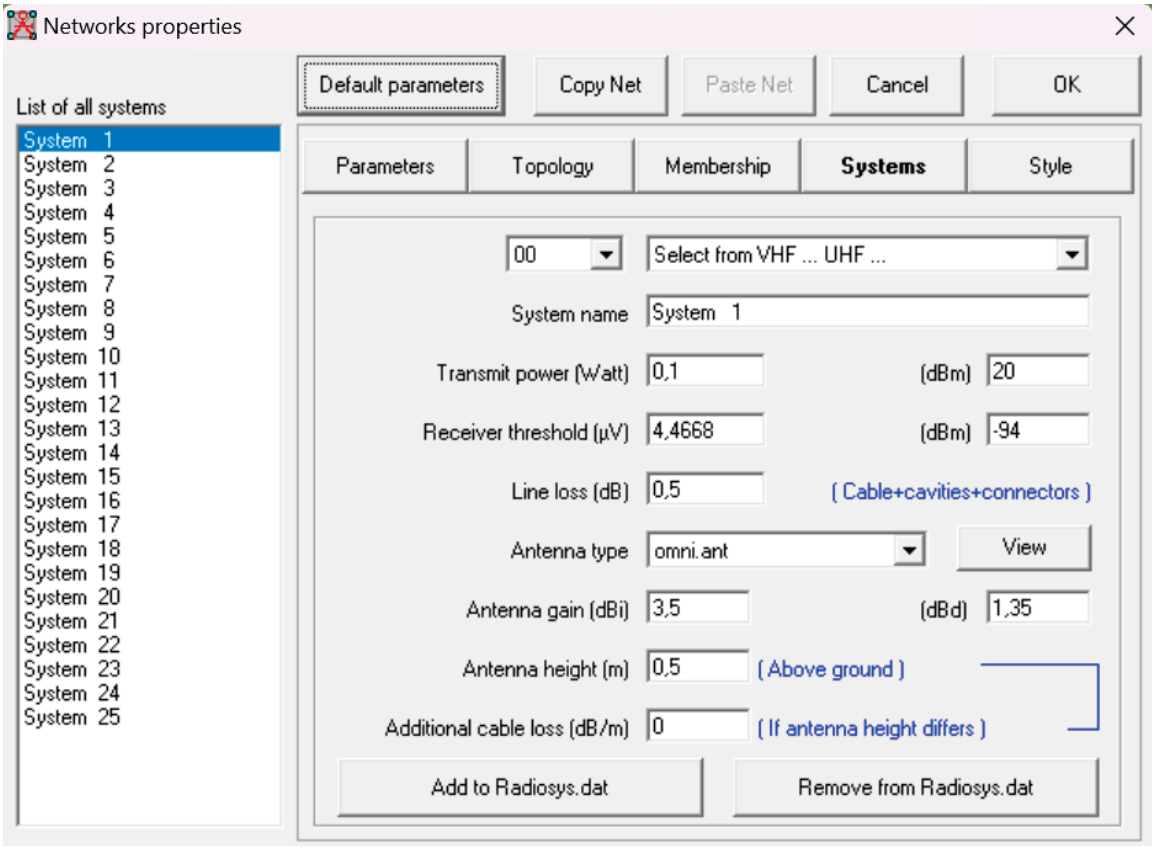


SOURCE: The Author.

the city of Ingolstadt, the drone controller was positioned on top of a 17-meter-high building. Consequently, for the simulation of the flight in Ingolstadt, the antenna height representing the controller was set to 17 meters in the Radio Mobile software to reflect the building's height.

All sampled latitude and longitude points were then entered into the software for communication link simulation, considering the information provided for modeling radio signal propagation in the specified areas using the Longley-Rice model in point-to-point prediction mode. FIGURE 11 exemplifies the simulation of a communication point in Radio Mobile.

Radio Mobile provides a range of information about the communication link, as shown in FIGURE 11 at the top. The Azimuth is the azimuth angle of the transmitter's antenna to the receiver, based on geographical coordinates. Pathloss quantifies the signal loss along the path between the two locations, in decibels, quantifying signal attenuation. The Elevation Angle is the elevation angle of the signal when transmitted from the transmitting antenna.

The E-field denotes the signal level measured in dB$\mu$V/m (decibels microvolt per meter), mainly used in transmission calculations and coverage mapping. Clearance refers to the distance from the signal path to any potential obstructions. The Rx Level,

FIGURE 11 – EXAMPLE OF POINT-TO-POINT COMMUNICATION IN RADIO MOBILE.


SOURCE: The Author.

expressed in dBm or $\mu V$, indicates the power at which the signal is received. Rx Relative presents the signal level above the receiver's threshold, effectively serving as a margin against signal fading along the transmission path. Information about the Fresnel zone and the distance between the transmitter and receiver, in kilometers, is also displayed in the Worst Fresnel and Distance fields.

Considering the signal strength measurement, the values for all sampled flight points calculated in the Rx Level field, in dBm, were accounted for to assign a result obtained from the Radio Mobile simulations.

For each flight point simulated in Radio Mobile, the Rx Level value is considered. The obtained values consider the transmitted signal power, inherent path losses, including attenuation due to distance, obstructions, and interferences that can affect signal quality. The results obtained from the Radio Mobile simulations are presented in the CHAPTER 4.

## 3.4 MULTILAYER PERCEPTRON

The development of the artificial neural network begins with the acquisition and preprocessing of flight telemetry data. The methodology includes stages of modeling,

training, validation, testing, and inference of the multilayer perceptron. For the implementation of the algorithm, the PyTorch framework was used, a library widely adopted in machine learning and computer vision applications.

The neural network is structured as a fully connected multilayer perceptron, consisting of three layers: input, hidden, and output. The input layer has ten nodes, while the output layer has a single node corresponding to the Wi-Fi signal strength.

For the selection of the neural network input parameters, a correlation matrix was employed to identify the variables that illustrate the highest correlation with the signal strength values present in the 'wifi_signal' column. This process aims at dimensionality reduction and the detection of multicollinearity among the variables.

The correlation matrix was obtained through Pearson's correlation coefficient, which measures the linear correlation between two continuous variables. Correlation values range from -1 to 1, where 1 indicates perfect positive correlation, -1 indicates perfect negative correlation, and 0 indicates no correlation between the variables.

Considering a correlation threshold of 0.70 in absolute value with the signal strength data, the following were chosen as input parameters for the neural network: terrain type ('landcover'), altitude ('gps_amsl_altitude'), elevation angle ('angle_phi', 'angle_psi', and 'angle_theta'), speed ('speed_vx', 'speed_vy', and 'speed_vz'), battery percentage ('battery_percent'), and distance between the drone and the controller ('distance_to_base').

Collecting time-series received signal strength (RSS) observations and averaging them is a common practice to manage RSS fluctuations. However, this approach is compromised by the presence of outliers in the observations, which significantly impact the averaging process and reduce its efficiency. To address this issue, the Z-score method, based on the median absolute deviation scale estimator, has been used to detect outliers (Yaro et al., 2024).

For this project, Z-score normalization was selected to minimize the impact of outliers, providing a more robust and accurate representation of the RSS data. The selected normalization method ensures that the values of columns such as altitude, elevation angle, terrain type, distance between the drone and the controller, speed, and battery percentage are normalized to have a mean of zero and a standard deviation of one. This method ensures that the data share a common scale before being used for training and testing the neural network.

The following equation illustrates the application of Z-normalization:

$$z = \frac{x - \mu}{\sigma}, \tag{3.9}$$

where $x$ is the original value, $\mu$ is the mean of the values, and $\sigma$ is the standard deviation.

The hyperparameter configuration was defined through an exhaustive grid search using the 'GridSearchCV' tool from 'scikit-learn'. The objective of the hyperparameter search is to identify the optimal parameters to maximize the model's performance. The tested combinations include the number of neurons in the hidden layer ranging from 10 to 40, optimizers (ADAM, SGD, and NAdam), and activation functions (ReLU, sigmoid, and hyperbolic tangent), with learning rates varying between 0.1 and 0.0001.

The results of the exhaustive grid search indicated the ideal hyperparameters for the MLP as shown in TABLE 5.

TABLE 5 – HYPERPARAMETERS CONSIDERED IN THE MLP MODELING.

| **Metric** | **Value** |
|---|---|
| Number of Neurons | 10 |
| Optimizer | Adam |
| Activation Function | Sigmoid |
| Learning Rate | 0.01 |

SOURCE: The Author.

The dataset was partitioned so that 70% (27.884 samples) were used for training, 20% (7.967 samples) for validation, and 10% (3.983 samples) for test. This division maintains the proportional representation of the regions under analysis. The supervised training of the network used the backpropagation method for 500 epochs, similar to what was done in the research by Saadi et al. (2022). Additionally, the early stopping process is implemented to prevent overfitting, terminating the training when the validation loss begins to increase after 100 consecutive epochs.

The training phase of the multilayer perceptron was executed twenty times, with average values computed to find the best training and validation loss values. The weights were randomly initialized using the 'randn' function from PyTorch, which is used to generate tensors filled with random numbers from a Gaussian distribution with mean zero and standard deviation one. The loss function used was MSELoss as given in **??**.

Additionally, three-fold cross-validation was employed to ensure the model's robustness. In this method, the dataset is randomly divided into three approximately equal-sized subsets (or folds). In each of the three iterations, two subsets are used for training and the third is used for validation. The model's final performance is evaluated by the average performance across the three iterations, providing a more reliable estimate of the model's generalization capability.

To perform inference with the previously trained neural network, data from the same three flights in rural, suburban, and urban regions, previously used in the simulations employing the Longley-Rice model, were utilized. At this stage, the data

used had not been presented to the neural network during the training process, thus allowing the evaluation of its effectiveness with new and unknown data.

The final signal strength values obtained from the neural network inference were denormalized and then compared with the expected results, i.e., those derived from the telemetry data collected during the drone flights. This comparison is crucial to verify the model's accuracy under real operating conditions, allowing the assessment of whether the neural network's predictions reflect the measurements taken during the flights. Subsequently, the MLP results were compared with the values obtained from the simulations in the Radio Mobile software using the Longley-Rice terrain model.

# 4 RESULTS

## 4.1 RESULTS OF THE SIMULATIONS IN RADIO MOBILE

To quantify the accuracy of the simulation results obtained with the Radio Mobile software, the relative error, RMSE, and MAE values were calculated.

The relative error was obtained using the following relation:

$$\text{Relative Error} = \frac{1}{n}\sum_{i=1}^{n}\frac{|\hat{Y}_i - Y_i|}{|Y_i|}, \tag{4.1}$$

where $n$ represents the total number of samples, $\hat{Y}_i$ is the received power value for the $i$-th simulated sample, and $Y_i$ is the received power value for the $i$-th telemetry sample.

For the RMSE results, EQUATION 2.9 was used, where $n$ represents the total number of observations, $Y_i$ is the value measured by the drone for the $i$-th data point, and $\hat{Y}_i$ is the value predicted by the model. For the MAE results, EQUATION 2.10 was used.

The results obtained with the simulation in Radio Mobile using the Longley-Rice terrain model considering the three flights with different levels of urbanization are shown in TABLE 6.

TABLE 6 – ERROR METRICS BY REGION USING LONGLEY-RICE MODEL

| Flight | Relative Error (dB) | RMSE (dB) | MAE (dB) |
|---|---|---|---|
| Rural region | 5.05 | 8.23 | 6.04 |
| Suburban region | 8.16 | 10.88 | 8.74 |
| Urban region | 11.54 | 12.84 | 11.31 |

SOURCE: The Author.

In the rural region, the data indicate the lowest values for relative error, RMSE, and MAE among the regions. This result indicates higher accuracy in the simulations conducted in this area, implying a smaller variation and deviation of the values obtained with the Longley-Rice model compared to the actual values measured during the drone flight.

For the suburban region, the results exhibit an intermediate relative error, RMSE and MAE values when compared to the rural and urban regions, reflecting a balance between the characteristics of rural and urban environments.

In contrast, the urban region exhibits the highest relative error, RMSE, and MAE values among the analyzed areas, reflecting lower accuracy in this region's

measurements. This outcome is likely due to the higher levels of signal interference prevalent in urban scenarios.

FIGURE 12, FIGURE 13, and FIGURE 14 illustrate the results obtained considering the distance between the receiver and the transmitter.

FIGURE 12 – RESULTS OBTAINED WITH THE LONGLEY-RICE MODEL FOR THE RURAL REGION.

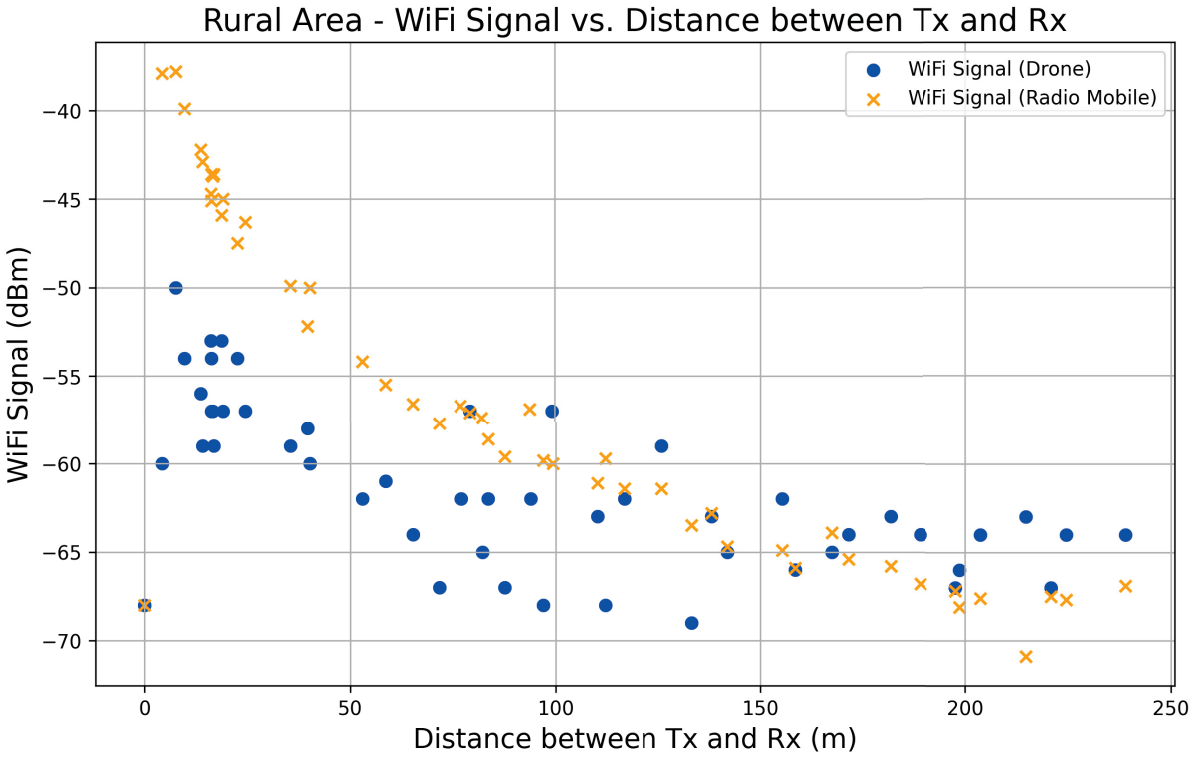


SOURCE: The Author.

In the rural region, it is observed that the signal strength decreases with increasing distance in both the measured and simulated values. This is expected, considering the characteristics of signal propagation and the decay of received power with distance. Additionally, the data obtained through the simulation with the Longley-Rice model exhibits reduced dispersion, indicating consistency in the model used due to the nature of the rural environment. Specifically, the MAE is 6.04 dB, which indicates a relatively small average deviation of the predicted values from the actual values. The rural environment has fewer elements that contribute to signal interference, resulting in more stable and predictable transmission quality.

In the suburban region, it is noted that the variation of the signal strength points simulated by the Radio Mobile software is more pronounced than that observed in the rural region, indicating the presence of more elements causing interference in this area. Such interferences result from the nature of the suburban environment, which, although not as densely urbanized as an urban region, still has a sufficient number of obstacles,

FIGURE 13 – RESULTS OBTAINED WITH THE LONGLEY-RICE MODEL FOR THE SUBURBAN REGION.

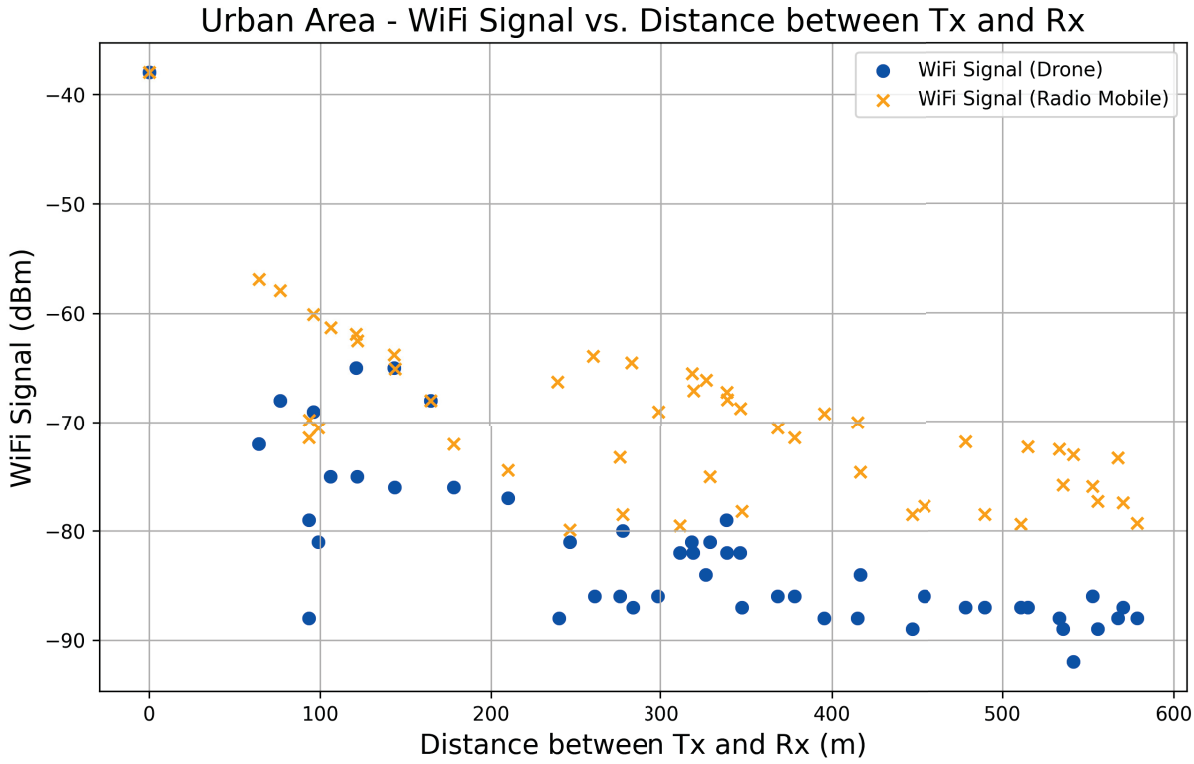


SOURCE: The Author.

such as smaller buildings, vegetation, and varied topography, which can affect signal propagation and, consequently, its received power.

In the urban region, it is found that the decline in signal strength as a function of distance is more gradual compared to other regions, which is associated with urban topography that tends to influence the signal behavior more uniformly. The results obtained with Radio Mobile showed significant differences when compared to the power received data measured by the drone, reflecting the limitations of the Longley-Rice model in accurately predicting all interference variables inherent to the urban environment.

In all regions, the received power decreases with increasing distance, which is a standard behavior due to signal attenuation with distance. It was observed that the results obtained with the Longley-Rice model through the Radio Mobile software diverged from the telemetry data obtained from the drone flights for the three scenarios, highlighting the importance of developing more robust and comprehensive methodologies for predicting received power in communication signals. In this context, the application of artificial neural networks emerges as a promising solution for signal strength prediction problems in environments characterized by different types of urbanization.

FIGURE 14 – RESULTS OBTAINED WITH THE LONGLEY-RICE MODEL FOR THE URBAN REGION.

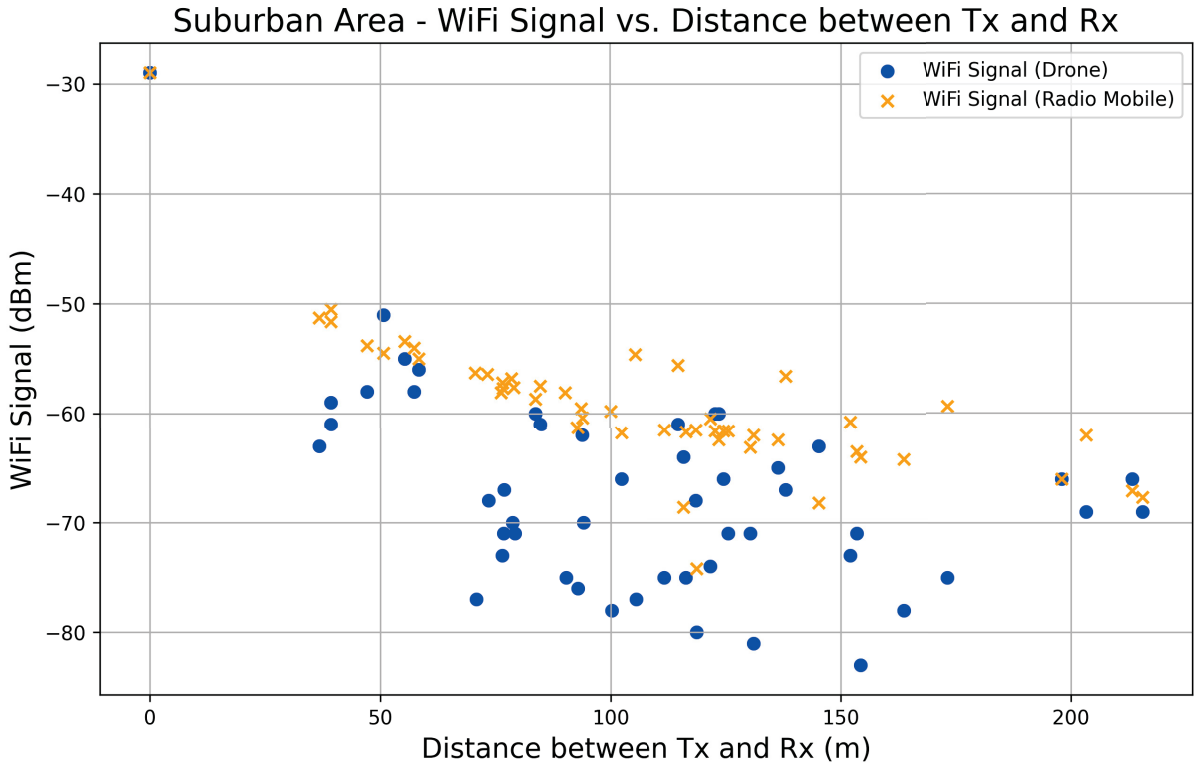


SOURCE: The Author.

## 4.2 RESULTS OF THE MULTILAYER PERCEPTRON

After training, an average validation loss of 0.24 and a training loss of 0.18 were obtained. The small difference between the training and validation loss values is a positive indicator of the model's ability to generalize to unseen data.

Considering the results obtained from the inference after training the neural network, the RMSE and MAE values for the three regions are shown in TABLE 7.

TABLE 7 – ERROR METRICS BY REGION USING MLP.

| Region | RMSE (dB) | MAE (dB) |
|---|---|---|
| Rural region | 1.95 | 9.89 |
| Suburban region | 2.93 | 7.77 |
| Urban region | 2.39 | 7.99 |

SOURCE: The Author.

The MLP model demonstrates varying levels of performance depending on the geographical region. Specifically, in the rural region, the model exhibits the lowest RMSE, indicating less variation in the prediction errors. However, this same region exhibits the highest MAE, suggesting that the average errors are higher. In contrast,

in the suburban region, the model has the highest RMSE, indicating greater variation in the prediction errors, but it presents the lowest MAE, indicating that the average errors are smaller. Finally, the urban region exhibits intermediate performance regarding both RMSE and MAE, positioning itself between the values observed in the rural and suburban regions.

In comparison with the findings of Saadi et al. (2022), who implemented an ANN model to predict signal strength at varying altitudes with a reported accuracy of 97%, the performance achieved by the MLP developed in this research is similarly robust. While their ANN achieved low MSE values (3.91% at 10 meters, 4.20% at 18 meters, and 4.51% at 24 meters) the MLP developed in this research demonstrated an average RMSE of 1.95 dB for rural environments, 2.93 dB for suburban areas, and 2.39 dB for urban areas. These results align closely with the performance metrics of Saadi et al. (2022) and suggest that the MLP developed in this research achieves comparable accuracy across various environments, despite differences in input features and specific network architectures.

Furthermore, when comparing with the findings of Eichie et al. (2017), who examined both conventional models (Okumura-Hata, Egli, COST-231, and Ericsson) and an ANN-based approach, similar improvements over traditional models are observed. For rural and suburban settings, the ANN outperformed theoretical models, with Eichie et al. (2017) reporting optimal RMSE values between 3.96 and 7.07 dB for rural routes and between 1.22 and 6.16 dB for suburban routes. The results achieved by the MLP developed in this research—1.95 dB for rural, 2.93 dB for suburban, and 2.39 dB for urban environments—further confirm the enhanced accuracy of ANN-based models over traditional approaches, aligning with the findings of Eichie et al. (2017) and highlighting the model's efficacy for signal strength prediction across various environmental conditions.

## 4.3 COMPARISON OF MULTILAYER PERCEPTRON AND LONGLEY-RICE MODEL RESULTS

The MLP results were compared with the values obtained from simulations in the Radio Mobile software using the Longley-Rice terrain model and with the values measured with the drone. FIGURE 15, FIGURE 16, and FIGURE 17 illustrate the received signal strength values obtained for rural, suburban, and urban regions.

For the rural area, there is a noticeable trend of decreasing Wi-Fi signal intensity as the distance from the base increases, which is expected due to signal attenuation with distance. In the first 50 meters, there is a significant variation between the measured values and those predicted by the Longley-Rice model. Specifically, the values obtained from the Radio Mobile simulation overestimate the received power, while the data

FIGURE 15 – SIGNAL STRENGTH AS A FUNCTION OF DISTANCE FOR THE RURAL REGION.

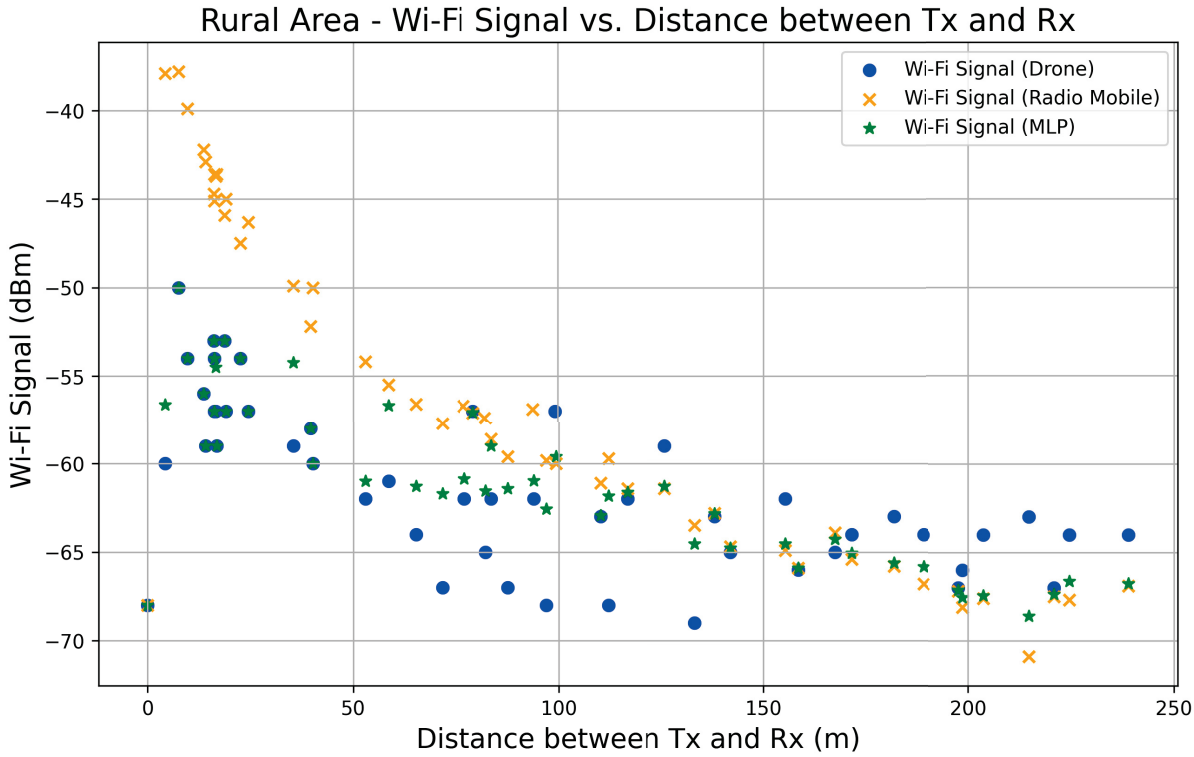


SOURCE: The Author.

measured by the drone indicate the presence of possible obstacles and interferences in the first meters of the flight, factors not considered by the Longley-Rice model. Beyond 50 meters, the predictions of the Longley-Rice model and the measured values converge.

On the other hand, the signal intensity predictions made by the multilayer perceptron align more closely with the actual values measured by the drone, demonstrating greater accuracy in relation to the real data. From 100 meters onward, both models, Longley-Rice and multilayer perceptron, exhibit better correspondence with the real data, although some variations are still observed. However, the model proposed by the multilayer perceptron offers superior correspondence with the measured data compared to the Longley-Rice terrain model.

In the suburban area, comparing the drone's actual measurements to the signal strength predicted by the Radio Mobile model using Longley-Rice, it is shown that these predictions follow the general trend of the measured data but exhibit a slightly different pattern. The discrepancies may arise from the model's inherent assumptions and simplifications, which do not fully capture the actual environmental complexity.

The predicted signal strength from the multilayer perceptron also follows the

FIGURE 16 – SIGNAL STRENGTH AS A FUNCTION OF DISTANCE FOR THE SUBURBAN REGION.

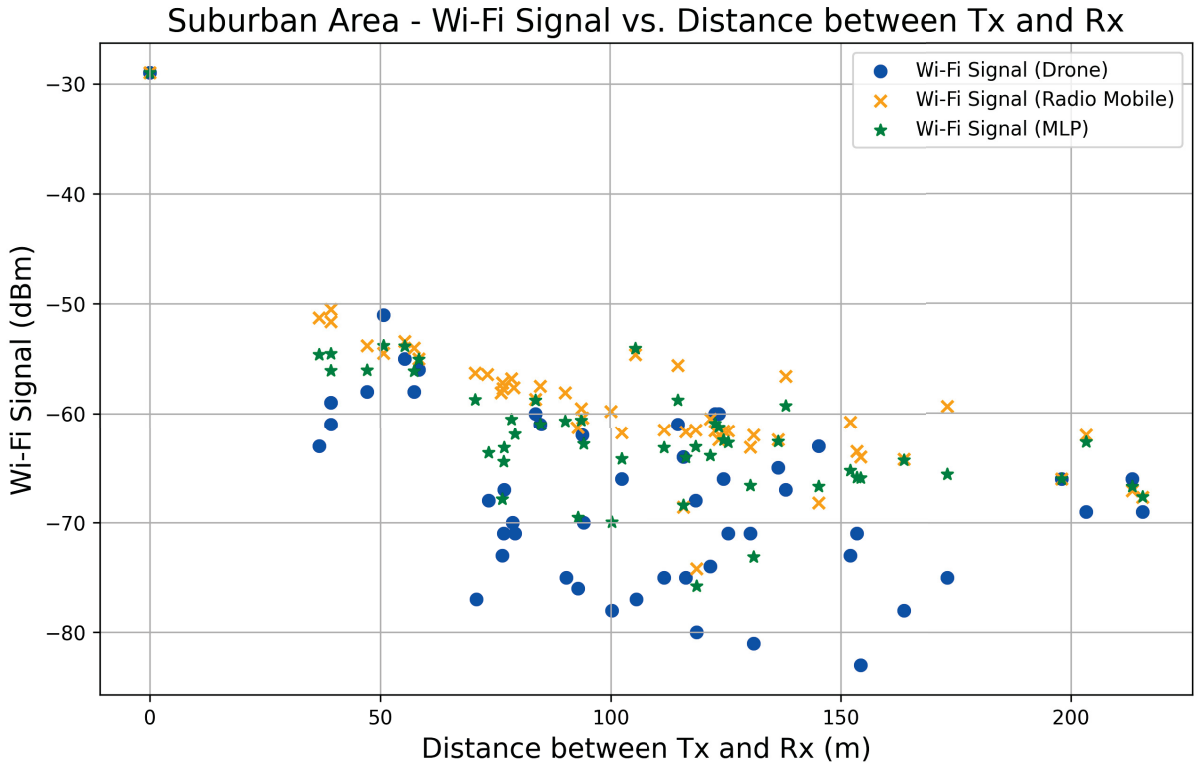


SOURCE: The Author.

trend of decreasing signal strength with increasing distance and appears to align more closely with the actual drone measurements than the Radio Mobile predictions.

The actual drone measurements exhibit greater variability compared to the predicted datasets. This variability likely stems from real-world environmental factors that the prediction models do not account for, such as buildings, trees, and other obstacles causing signal reflections and scattering.

When comparing the predictions, the signal strength predicted by the multilayer perceptron matches the actual data more closely than the values predicted by the Longley-Rice model. This suggests that the multilayer perceptron prediction method may be more accurate or better suited for this suburban environment.

For the urban area, the measured Wi-Fi signal demonstrates significant variability, characterized by substantial fluctuations in signal strength across all distances. This variability can be attributed to environmental factors prevalent in urban settings, such as buildings, trees, and other obstacles.

The predictions from the Radio Mobile model also indicate a decrease in signal strength with increasing distance. However, the Radio Mobile model tends to overestimate the signal strength compared to the actual drone measurements. Beyond 100

FIGURE 17 – SIGNAL STRENGTH AS A FUNCTION OF DISTANCE FOR THE URBAN REGION.

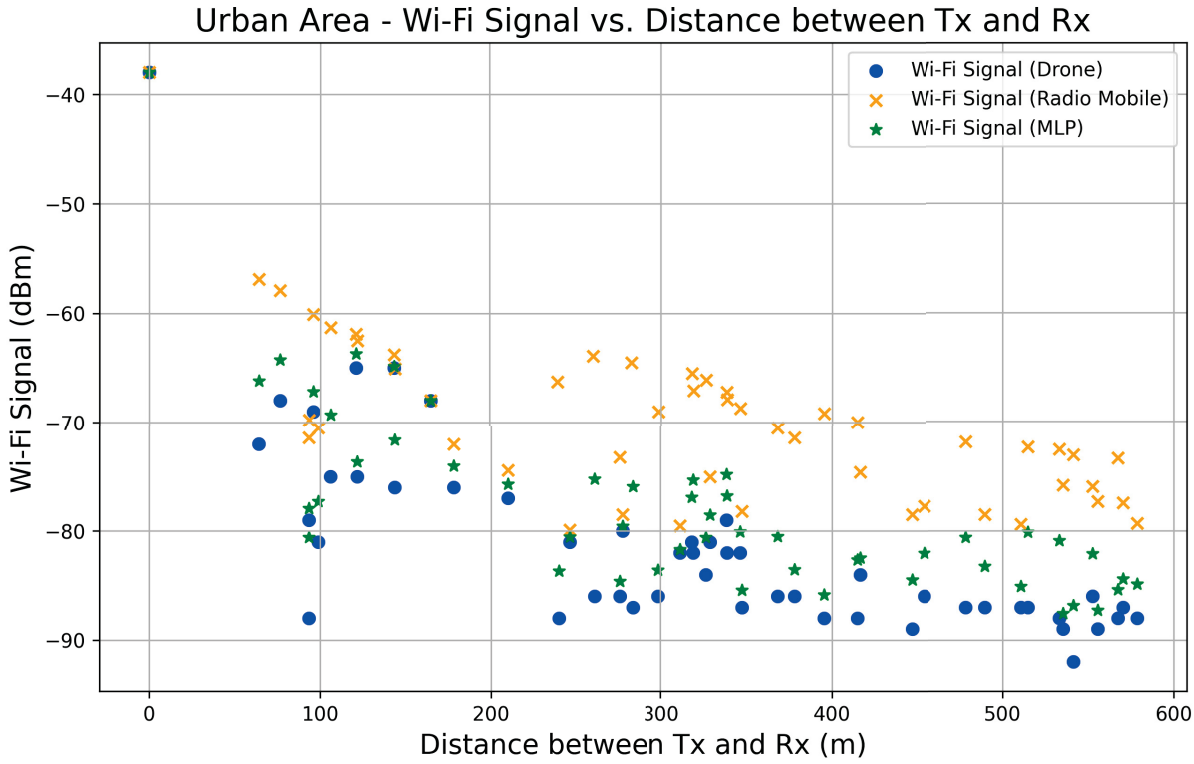


SOURCE: The Author.

meters, the model generally predicts higher signal strengths than the actual measurements, although both trends decline with distance.

The multilayer perceptron predictions closely follow the general trend of the actual measurements more accurately than the Longley-Rice model. While discrepancies still exist, this model appears to be more accurate or account for more real-world urban environmental variables.

The actual Wi-Fi signal measurements exhibit significant variability, likely due to urban obstructions. The Longley-Rice model generally overestimates signal strength across all distances. In contrast, the multilayer perceptron model aligns more closely with the actual drone measurements, albeit with a slight tendency to overestimate signal strength. For practical applications, the multilayer perceptron model provides a more realistic prediction of Wi-Fi signal strength in urban areas compared to the Longley-Rice model.

The comparative analysis between Wi-Fi signal strength prediction models reveals that the multilayer perceptron model aligns more closely with the real values measured by drones compared to the Longley-Rice model. While the Longley-Rice model tends to overestimate signal strength, the multilayer perceptron model exhibits a

more accurate correspondence with the real measurements, despite also displaying a slight tendency to overestimate.

The real drone measurements exhibit significant variability due to interferences and obstructions such as buildings and trees, which are not fully captured by the predictive models. Therefore, the multilayer perceptron model is more suitable for predicting Wi-Fi signal strength in the three regions, as it better captures the complexities and environmental variations typical of the analyzed areas, adjusting more precisely to the changes in signal strength caused by physical obstacles and interferences present in the environment.

# 5 CONCLUSION AND FUTURE WORK

The observed discrepancies between the outcomes generated by the Longley-Rice model, implemented through the Radio Mobile software, and the telemetry data acquired from drone flights across three distinct scenarios underscore the necessity of developing more accurate methodologies for predicting signal strength during drone flights. In this context, the application of artificial intelligence techniques emerges as an alternative for scenarios involving the prediction of signal strength in drone flights.

The signal intensity values obtained with the multilayer perceptron, presented in TABLE 7, indicate that in the rural region, the RMSE is 1.95 dB, suggesting a lower variation in prediction errors. In contrast, the signal intensity values obtained with the Longley-Rice model, shown in TABLE 6, indicate a significantly higher RMSE of 8.23 dB for the same region, indicating a greater variation in prediction errors.

For the suburban region, the multilayer perceptron presents an RMSE of 2.93 dB, indicating greater variation in prediction errors compared to the rural region. In turn, the Longley-Rice model shows an RMSE of 10.88 dB, a considerably higher value than the RMSE observed with the multilayer perceptron.

In the urban region, the multilayer perceptron demonstrates an RMSE of 2.39 dB, while the Longley-Rice model presents an RMSE of 12.84 dB, the highest among all analyzed regions. This RMSE difference indicates that the Longley-Rice model has a greater variation in prediction errors compared to the multilayer perceptron.

In conclusion, the RMSE values obtained through the two methodologies highlight a significant discrepancy, with the Longley-Rice model consistently presenting higher values for all regions. This disparity suggests that the Longley-Rice model's predictions overestimate the received power values by not adequately considering the signal interferences and obstructions present in the analyzed regions.

For future work, it is recommended to obtain a more robust and varied dataset, covering a larger number of regions and environments, in order to enhance the generalization of the multilayer perceptron algorithm. Additionally, it is suggested to use machine learning methods such as Random Forest or Support Vector Machine, which are more suitable for scenarios with high noise presence. Another possibility for future work is to employ the signal intensity prediction algorithm in scenarios of optimization and prediction of drone flight trajectories, aiming to maximize available resources and promote energy efficiency during UAV operations.

# REFERENCES

ALSAMHI, S. H.; MA, O.; ANSARI, M. S. **Predictive Estimation of the Optimal Signal Strength from Unmanned Aerial Vehicle over Internet of Things Using ANN**. [S.l.: s.n.], 2018. arXiv: 1805.07614 [eess.SP]. Cited on pages 19, 20, 22.

BEHJATI, M.; MOHD NOH, A. B.; ALOBAIDY, H. A. H.; ZULKIFLEY, M. A.; NORDIN, R.; ABDULLAH, N. F. LoRa Communications as an Enabler for Internet of Drones towards Large-Scale Livestock Monitoring in Rural Farms. **Sensors**, v. 21, n. 15, 2021. ISSN 1424-8220. DOI: 10.3390/s21155044. Available at: https://www.mdpi.com/1424-8220/21/15/5044. Cited on pages 17, 22.

CHENG, X.; LI, Y.; BAI, L. UAV Communication Channel Measurement, Modeling, and Application. **Journal of Communications and Information Networks**, v. 4, n. 4, p. 32–43, 2019. DOI: 10.23919/JCIN.2019.9005432. Cited on pages 5, 7.

CYBENKO, G. V. Approximation by superpositions of a sigmoidal function. **Mathematics of Control, Signals and Systems**, v. 2, p. 303–314, 1989. Available at: https://api.semanticscholar.org/CorpusID:3958369. Cited on page 14.

DELISLE, G.; LEFEVRE, J.-P.; LECOURS, M.; CHOUINARD, J.-Y. Propagation Loss Prediction: A Comparative Study with Application to the Mobile Radio Channel. **Vehicular Technology, IEEE Transactions on**, p. 86–96, jun. 1985. DOI: 10.1109/T-VT.1985.24041. Cited on page 9.

EICHIE, J.; OYEDUM, O.; AJEWOLE, O.; AIBINU, A. Comparative analysis of basic models and artificial neural network based model for path loss prediction. **Progress In Electromagnetics Research M**, v. 61, p. 133–146, jan. 2017. DOI: 10.2528/PIERM17060601. Cited on pages 11, 20–22, 42.

HAYKIN, S. **Neural networks and learning machines**. 3. ed. [S.l.]: Prentice Hall, 2008. Includes bibliographical references and index. ISBN 978-0-13-147139-9. Cited on pages 12, 14, 15.

HUFFORD, G. A.; LONGLEY, A. G.; KISSICK, W. A. A Guide to the Use of the ITS Irregular Terrain Model in the Area Prediction Mode. In. Available at: https://api.semanticscholar.org/CorpusID:128452808. Cited on pages 8, 9.

KOSZTRA, B.; BÜTTNER, G.; HAZEU, G.; ARNOLD, S. **Updated CLC illustrated nomenclature guidelines**. [S.l.: s.n.], mai. 2019. Available at: https://land.copernicus.eu/en/technical-library/clc-illustrated-nomenclature-guidelines/@@download/file. Cited on pages 26, 28.

LAHMERI, M.-A.; KISHK, M. A.; ALOUINI, M.-S. Artificial Intelligence for UAV-Enabled Wireless Networks: A Survey. **IEEE Open Journal of the Communications Society**, v. 2, p. 1015–1040, 2021. DOI: 10.1109/OJCOMS.2021.3075201. Cited on pages 2, 11.

MITCHELL, T. **Machine Learning**. [S.l.]: McGraw-Hill Education, 1997. (McGraw-Hill international editions - computer science series). ISBN 9780070428072. Available at: https://books.google.de/books?id=xOGAngEACAAJ. Cited on pages 11, 16.

PARK, C.; TETTEY, D. K.; JO, H.-S. **Artificial Neural Network Modeling for Path Loss Prediction in Urban Environments**. [S.l.: s.n.], 2019. arXiv: 1904.02383 [cs.LG]. Cited on pages 18, 19, 22.

PARROT DRONE, S. **Anafi AI User Guide v7.5.0.0**. Accessed in: 17/06/2024. 2023. Available at: https://www.parrot.com/assets/s3fs-public/2022-07/ANAFI%20Ai%20USER%20GUIDE%20v.7.3.0.0_0.pdf. Cited on page 23.

PHILLIPS, C.; SICKER, D.; GRUNWALD, D. A Survey of Wireless Path Loss Prediction and Coverage Mapping Methods. **IEEE Communications Surveys  Tutorials**, v. 15, n. 1, p. 255–270, 2013. DOI: 10.1109/SURV.2012.022412.00172. Cited on pages 5–8.

POPESCU, I.; NIKITOPOULOS, D.; CONSTANTINOU, P.; NAFORNITA, I. ANN Prediction Models for Outdoor Environment. In: 2006 IEEE 17th International Symposium on Personal, Indoor and Mobile Radio Communications. [S.l.: s.n.], 2006. P. 1–5. DOI: 10.1109/PIMRC.2006.254270. Cited on page 15.

RAMCHOUN, H.; AMINE, M.; IDRISSI, J.; GHANOU, Y.; ETTAOUIL, M. Multilayer Perceptron: Architecture Optimization and Training. **International Journal of Interactive Multimedia and Artificial Inteligence**, v. 4, p. 26–30, jan. 2016. DOI: 10.9781/ijimai.2016.415. Cited on page 14.

RAMCHOUN, H.; IDRISSI, M. A. J.; GHANOU, Y.; ETTAOUIL, M. Multilayer Perceptron: Architecture Optimization and Training. **Int. J. Interact. Multim. Artif. Intell.**, v. 4, p. 26–30, 2016. Cited on pages 13–15.

SAADI, I. A.; TARHUNI, N.; MESBAH, M. Ground Level Mobile Signal Prediction Using Higher Altitude UAV Measurements and ANN. In: 2022 32nd Conference of Open Innovations Association (FRUCT). [S.l.: s.n.], 2022. P. 15–21. DOI: 10.23919/FRUCT56874.2022.9953813. Cited on pages 17, 22, 36, 42.

SHAKOOR, S.; KALEEM, Z.; BAIG, M. I.; CHUGHTAI, O.; DUONG, T. Q.; NGUYEN, L. D. Role of UAVs in Public Safety Communications: Energy Efficiency Perspective. **IEEE Access**, v. 7, p. 140665–140679, 2019. DOI: 10.1109/ACCESS.2019.2942206. Cited on page 2.

YANG, G.; ZHANG, Y.; HE, Z.; WEN, J.; JI, Z.; LI, Y. Machine-Learning-Based Prediction Methods for Path Loss and Delay Spread in Air-to-Ground Millimeter Wave Channels. **IET Microwaves, Antennas  Propagation**, v. 13, jul. 2019. DOI: 10.1049/iet-map.2018.6187. Cited on page 2.

YARO, A. S.; MALY, F.; PRAZAK, P.; MALÝ, K. Outlier Detection Performance of a Modified Z-Score Method in Time-Series RSS Observation With Hybrid Scale Estimators. **IEEE Access**, v. 12, p. 12785–12796, 2024. DOI: 10.1109/ACCESS.2024.3356731. Cited on page 35.

ZENG, Y.; ZHANG, R.; LIM, T. J. Wireless communications with unmanned aerial vehicles: opportunities and challenges. **IEEE Communications Magazine**, v. 54, n. 5, p. 36–42, 2016. DOI: 10.1109/MCOM.2016.7470933. Cited on page 2.